

Style Definition: Comment Text

1 **Relative Importance of High-Latitude Local and Long-Range**
2 **Transported Dust to Arctic Ice Nucleating Particles and Impacts**
3 **on Arctic Mixed-Phase Clouds**

4 Yang Shi¹, Xiaohong Liu¹, Mingxuan Wu², Xi Zhao¹, Ziming Ke¹, and Hunter Brown¹

5 ¹Department of Atmospheric Sciences, Texas A&M University, College Station, TX, USA

6 ²Atmospheric Sciences and Global Change Division, Pacific Northwest National Laboratory,
7 Richland, WA, USA

8

9 *Correspondence to:* Xiaohong Liu (xiaohong.liu@tamu.edu)

10

11 **Abstract.** Dust particles, serving as ice nucleating particles (INPs), may impact the Arctic surface
12 energy budget and regional climate by modulating the mixed-phase cloud properties and lifetime.
13 In addition to long-range transport from low latitude deserts, dust particles in the Arctic can
14 originate from local sources. However, the importance of high latitude dust (HLD) as a source of
15 Arctic INPs (compared to low latitude dust (LLD)) and its effects on Arctic mixed-phase clouds
16 are overlooked. In this study, we evaluate the contribution to Arctic dust loading and INP
17 population from HLD and six LLD source regions by implementing a source-tagging technique
18 for dust aerosols in version 1 of the US Department of Energy's Energy Exascale Earth System
19 Model (E3SMv1). Our results show that HLD is responsible for 30.7% of the total dust burden in
20 the Arctic, whereas LLD from Asia and North Africa contribute 44.2% and 24.2%, respectively.
21 Due to its limited vertical transport as a result of stable boundary layers, HLD contributes more in
22 the lower troposphere, especially in boreal summer and autumn when the HLD emissions are
23 stronger. LLD from North Africa and East Asia dominates the dust loading in the upper
24 troposphere with peak contributions in boreal spring and winter. The modeled INP concentrations
25 show a better agreement with both ground and aircraft INP measurements in the Arctic when
26 including HLD INPs. The HLD INPs are found to induce a net cooling effect (-0.24 W m^{-2} above
27 60°N) on the Arctic surface downwelling radiative flux by changing the cloud phase of the Arctic
28 mixed-phase clouds. The magnitude of this cooling is larger than those induced by North African
29 and East Asian dust (0.08 and -0.06 W m^{-2} , respectively), mainly due to different seasonalities of
30 HLD and LLD. Uncertainties of this study are discussed, which highlights the importance of
31 further constraining the HLD emissions.

32

33 1 Introduction

34 The Arctic has experienced long-term climate changes, including rapid warming and shrinking
35 in sea ice extent. Arctic mixed-phase clouds (AMPCs), which occur frequently throughout the year,
36 strongly impact the surface and atmospheric energy budget and are one of the main components
37 driving the Arctic climate (Morrison et al., 2012; Shupe and Intrieri, 2004; Tan and Storelvmo,
38 2019). The AMPCs lifetime, properties, and radiative effects are closely connected to the primary
39 ice formation process, as the formed ice crystals grow at the expense of cloud liquid droplets due
40 to the lower saturation vapor pressure with respect to ice than that to liquid water (so-called
41 Wegener-Bergeron-Findeisen process or, in short, WBF process; Liu et al., 2011; M. Zhang et al.,
42 2019). Large ice crystals with higher fall speeds than liquid droplets can readily initiate
43 precipitation and further deplete cloud liquid through the riming process. All these processes can
44 also interact with each other nonlinearly and impact the phase partitioning of mixed-phase clouds
45 (Tan and Storelvmo, 2016).

46 Primary ice formation in mixed-phase clouds only occurs heterogeneously with the aid of ice
47 nucleating particles (INPs). According to Vali et al. (1985), the heterogeneous ice nucleation is
48 classified into four different modes: through the collision of an INP particle with supercool liquid
49 droplet (contact freezing), by an INP particle immersed in a liquid droplet (immersion freezing),
50 when the INP particle also serves as a cloud condensation nucleus (condensation freezing), or by
51 the direct deposition of water vapor to a dry INP particle (deposition nucleation). The immersion
52 freezing is usually treated together with condensation freezing in models, as instruments cannot
53 distinguish between them (Vali et al., 2015). This immersion/condensation freezing is generally
54 thought to be the most important ice nucleation mode in the mixed-phase clouds (de Boer et al.,
55 2011; Prenni et al., 2009; Westbrook and Illingworth, 2013). It remains a significant challenge to

Deleted: through

Deleted: (WBF)

Deleted: (

59 characterize the INP types and concentrations, partially because only a very small fraction of
60 aerosols can serve as INPs (DeMott et al., 2010). This is especially the case for the clean
61 environment in the Arctic. Therefore, the potential sources and amounts of Arctic INPs are still
62 largely unknown.

63 Mineral dust aerosols are identified as one of the most important types of INPs in the atmosphere
64 due to their high ice nucleation efficiency (DeMott et al., 2003; Hoose and Möhler, 2012; Murray
65 et al., 2012; Atkinson et al., 2013) and their abundance in the atmosphere (Kinne et al., 2006).
66 They are mainly emitted from arid and semi-arid regions located at low- to mid-latitudes, such as
67 North Africa, the Middle East, and Asia. Observational studies found that LLD can be transported
68 to the Arctic (Bory et al., 2003; VanCuren et al., 2012; Huang et al., 2015) and act as a key
69 contributor to the Arctic INP population (Si et al., 2019). A modelling study also suggested that
70 low latitude dust (LLD) has a large contribution to dust concentrations in the upper troposphere of
71 the Arctic (Groot Zwaafink et al., 2016), since LLD is usually lifted by convection and topography
72 and then transported poleward following slantwise isentropes. This finding confirms the potential
73 of LLD to serve as INPs in AMPCs. The impact of LLD INPs on clouds was further investigated
74 by Shi and Liu (2019), who found that LLD INPs induce a net cooling cloud radiative effect in the
75 Arctic, due to their impacts on cloud water path and cloud fraction.

76 Although LLD has attracted much of the attention in the past, it is recognized that 2–3% of the
77 global dust emission is produced by local Arctic sources above 50°N (Bullard et al., 2016), which
78 include Iceland (Arnalds et al., 2016; Dagsson-Waldhauserova et al., 2014; Prospero et al., 2012),
79 Svalbard (Dörnbrack et al., 2010), Alaska (Crusius et al., 2011), and Greenland (Bullard and
80 Austin, 2011). Groot Zwaafink et al. (2016) found that high latitude dust (HLD) contributes 27%
81 of the total dust burden in the Arctic. Different from LLD, most of the emitted HLD is restricted

82 at the lower altitudes in the Arctic, because of the stratified atmosphere in the cold environment
83 (Bullard, 2017; Groot Zwaafink et al., 2016).

84 It is also noted that HLD is likely an important source to the observed INPs in the Arctic,
85 especially during the warm seasons. For example, Irish et al. (2019) suggested that mineral dust
86 from Arctic bare lands (likely eastern Greenland or north-western continental Canada) is an
87 important contributor to the INP population in the Canadian Arctic marine boundary layer during
88 summer 2014. Attempts have been made to quantify the ice nucleating ability of HLD. Paramonov
89 et al. (2018) found that the Icelandic glaciogenic silt had a similar ice nucleating ability as LLD at
90 temperatures below -30 °C. Similarly, Sanchez-Marroquin et al. (2020) suggested that the ice
91 nucleating ability of aircraft-collected Icelandic dust samples is slightly lower but comparable with
92 that of the LLD. Some other studies also noticed that HLD can act as efficient INPs at warm
93 temperatures. As early as the 1950s, the airborne dry dust particles from permafrost ground at
94 Thule, Greenland, were found to nucleate ice at temperatures as warm as -5 °C (Fenn and
95 Weickmann, 1959). This is corroborated by a more recent study which investigated the glacial
96 outwash sediments in Svalbard and ascribed the remarkably high ice nucleating ability to the
97 presence of soil organic matter (Tobo et al., 2019).

98 Despite their potential importance, HLD sources are largely underestimated or even omitted in
99 global models (Zender et al., 2003). Fan (2013) noticed that the autumn peak in measured surface
100 dust concentrations at Alert was underestimated by the model, likely due to a lack of local dust
101 emission. Similarly, Shi and Liu (2019) also mentioned that the distinction of simulated and
102 satellite retrieved dust vertical extinction in the Arctic became larger near the surface.

103 In this study, we account for the HLD dust emission by replacing the default dust emission
104 scheme (Zender et al., 2003) with the Kok et al. (2014a, b) scheme in the Energy Exascale Earth

105 System Model version 1 (E3SMv1). We further track explicitly the dust aerosols emitted from the
106 Arctic (HLD) and six major LLD sources using a newly developed source-tagging technique in
107 E3SMv1. The objectives of this study are to (1) examine the source attribution of the Arctic dust
108 aerosols in the planetary boundary layer and in the free troposphere; (2) examine the contribution
109 of dust from various sources to the Arctic dust INPs; and (3) quantify the subsequent influence of
110 dust INPs from various sources on the Arctic mixed-phase cloud radiative effects. We are
111 particularly interested in the relative importance of local HLD versus long-range transported LLD.

112 The paper is organized as follows. The E3SMv1 model and experiments setup are introduced in
113 Section 2. Section 3 presents model results and comparisons with observations. The uncertainties
114 are discussed in Section 4, and Section 5 summarizes the results.

115 **2 Methods**

116 **2.1 Model description and experiment setup**

117 Experiments in this study are performed using the atmosphere component (EAMv1) of the U.S.
118 Department of Energy (DOE) E3SMv1 model (Rasch et al., 2019). The model predicts number
119 and mass mixing ratios of seven aerosol species (i.e., mineral dust, black carbon (BC), primary
120 organic aerosol, secondary organic aerosol, sulfate, sea salt, and marine organic aerosol (MOA))
121 through a four-mode version of modal aerosol module (MAM4) (Liu et al., 2016; Wang et al.,
122 2020). The four aerosol modes are Aitken, accumulation, coarse, and primary-carbon modes, while
123 dust aerosols are carried in accumulation and coarse modes. Aerosol optical properties in each
124 mode is parameterized following Ghan and Zaveri (2007). The dust optics used in this study are
125 updated according to Albani et al. (2014).

126 EAMv1 includes a two-moment stratiform cloud microphysics scheme (MG2) (Gettelman and
127 Morrison, 2015). We note the WBF process rate in EAMv1 is tuned down by a factor of 10, which
128 results in more prevalent supercooled liquid water clouds in high latitudes than observations and
129 many other global climate models (Y. Zhang et al., 2019; Zhang et al., 2020). In addition, the
130 Cloud Layers Unified By Binormals (CLUBB) parameterization (Bogenschutz et al., 2013; Golaz
131 and Larson, 2002; Larson et al., 2002) is used to unify the treatments of planetary boundary layer
132 turbulence, shallow convection, and cloud macrophysics. Deep convection is treated by the Zhang
133 and McFarlane (1995) scheme.

134 In EAMv1, the heterogeneous ice nucleation in mixed-phase clouds follows the classical
135 nucleation theory (CNT) (Hoose et al., 2010; Y. Wang et al., 2014). CNT holds the stochastic
136 hypothesis, which treats the ice nucleation process as a function of time. Immersion/condensation,
137 contact, and deposition nucleation on dust and BC are treated in the CNT scheme. More details
138 about CNT parameterization are provided in Text S2.1 in the Supplement.

139 The experiments we conducted for this study are shown in Table 1. For the control experiment
140 (hereafter CTRL), the EAMv1 was integrated from July 2006 to the end of 2011 at 1° horizontal
141 resolution and 72 vertical layers. The first six months of the experiment were treated as model
142 spin-up and the last five-year results were used in analyses. The horizontal wind components were
143 nudged to the MERRA2 meteorology with a relaxation timescale of 6 hours (Zhang et al., 2014).
144 In addition to CTRL, we conducted three sensitivity experiments to investigate the INP effect of
145 dust from major source regions. In these sensitivity experiments, heterogeneous ice nucleation in
146 the mixed-phase clouds by dust from local Arctic sources, North Africa, and East Asia is turned
147 off (i.e., noArc, noNAf, and noEAs, respectively). The other settings of these three experiments
148 are identical to CTRL. Analyses related to the sensitivity experiments are provided in Section 3.4.

Deleted:), with the heterogenous ice nucleation in mixed-phase clouds following the classical nucleation theory (CNT) (Y.

Moved down [1]: Wang et al., 2014).

Moved down [2]: Immersion/condensation, contact, and deposition nucleation on dust and BC are treated in the CNT scheme. It should be noted

Deleted: It should be noted that

Moved (insertion) [1]

Moved (insertion) [2]

Deleted: is

Deleted: hour

Deleted:

159 2.2 Dust emission parameterization and source-tagging technique

Deleted: ¶

160 Dust emission in the default EAMv1 is parameterized following Zender et al. (2003) (Z03),
161 which uses semi-empirical dust source functions to address the spatial variability in soil erodibility.
162 The HLD emission is omitted in the Z03 scheme, since it was thought to be dubious (Zender et al.,
163 2003). In this study, we replaced the Z03 scheme with another dust emission parameterization
164 (Kok et al., 2014a, b) (K14) that avoids using a source function, [\(see more details about K14 in](#)
165 [Text S1\)](#). The K14 scheme is able to produce the HLD emission over Iceland, the Greenland coast,
166 Canada, Svalbard, and North Eurasia (Figure 1a). Furthermore, to address the overestimation in
167 dust emission in clay size ($< 2 \mu\text{m}$ diameter) (Kok et al., 2017), we changed the size distribution
168 of emitted dust particles from Z03 to that based on the brittle fragmentation theory (Kok, 2011).
169 1.1% of the total dust mass is emitted to the accumulation mode and 98.9% of that is emitted to
170 the coarse mode based on the brittle fragmentation theory, whereas the fractions are 3.2% and
171 96.8%, respectively in Z03.

Deleted: .

172 To quantify the source attribution of dust, we implemented a dust source-tagging technique in
173 EAMv1. This modeling tool was previously applied to BC (H. Wang et al., 2014; Yang et al.,
174 2017b), sulfate (Yang et al., 2017a), and primary organic aerosol (Yang et al., 2018) in the
175 Community Atmosphere Model version 5 (CAM5). [In this method, dust emission fluxes from](#)
176 [different sources are assigned to separate tracers and transport independently, so that dust](#)
177 originating from different sources can be tracked [and tuned separately](#) in a single model experiment.
178 As shown in Figure 1a, dust emissions from 7 source regions are tagged: Arctic (Arc; above 60°N ,
179 HLD source), North America (NA_m), North Africa (NA_f), Central Asia (CA_s), Middle East and
180 South Asia (MSA), East Asia (EA_s), and rest of the world (RoW). The Arctic source is further
181 divided into four sub-sources: Alaska (Ala), North Canada (NCa), Greenland and Iceland (GrI),

Deleted: With

Deleted: explicitly

186 and North Eurasia (NEu) (Figure S1), which are used in the analysis of INP sources in Section 3.3.
187 RoW represents the three major dust sources in the Southern Hemisphere (South America, South
188 Africa, and Australia), along with very low emissions from Europe and the Antarctic.

189 The global dust emission for CTRL is 5640 Tg yr^{-1} , which is tuned so that the global average
190 dust aerosol optical depth (DOD) is 0.031. This is within the range of the observational estimate
191 (0.030 ± 0.005) by Ridley et al. (2016). To maintain the magnitude of the global averaged DOD,
192 our tuned global dust emission exceeds the range of the AeroCom (Aerosol Comparisons between
193 Observations and Models) models (500 to 4400 Tg yr^{-1} ; Huneeus et al., 2011), likely due to a short
194 lifetime caused by too strong dust dry deposition at the bottom layer near the dust source regions
195 in EAMv1 (Wu et al., 2020). It is also about 2000 Tg yr^{-1} higher than the previous EAMv1 studies
196 (Shi and Liu, 2019; Wu et al., 2020), because we distribute less dust mass into the accumulation
197 mode and more dust mass into the coarse mode based on Kok (2011). The HLD emission is further
198 tuned up by 10 times so that it accounts for 2.6% (144 Tg yr^{-1}) of the global dust emission (Figure
199 1b), which is comparable with the recent estimates of 2-3% above 50°N by Bullard et al. (2016)
200 and of 3% above 60°N by Groot Zwaafink et al. (2016). The majority of global dust emission is
201 contributed from North Africa (51.9%, 2929 Tg yr^{-1}) and Asia (37.7%, 2124 Tg yr^{-1}), with Asian
202 emissions composed of MSA (20.2%, 1140 Tg yr^{-1}), EAs (10.9%, 613 Tg yr^{-1}), and CAs (6.6%,
203 371 Tg yr^{-1}). NAm has a weak dust emission of 33.4 Tg yr^{-1} that only contributes 0.6% to the
204 global emission, while the RoW has a combined contribution of 7.3% (410 Tg yr^{-1}). In addition,
205 the seasonal variations between HLD and LLD emissions are different - the HLD (Arctic) source
206 is more active in late summer and autumn, while the LLD sources (e.g., Naf, MSA, EAs) peak in
207 spring and early summer (Figure 1c).

208 **3 Result**

209 **3.1 Model validation**

210 To evaluate the model performance in simulating the dust cycle, we compare the model
211 predictions with measured aerosol optical depth (AOD), dust surface concentrations, and dust
212 deposition fluxes from global observation networks (Figure 2). We select and process the level 2.0
213 AOD data (2007-2011) at 40 “dust-dominated” ~~Aerosol RObotic~~ NETwork (AERONET; Holben
214 et al., 1998) stations following Kok et al. (2014b). We note that the AERONET AOD
215 measurements are biased towards clear-sky conditions due to the cloud-screening procedure
216 (Smirnov et al., 2000). For dust surface concentrations, we use the same measurements at 22 sites,
217 which Huneus et al. (2011) used for the AeroCom comparison, and further extend the dataset
218 with measurements at three high latitude stations: Heimaey (Prospero et al., 2012), Alert (~~Sirois~~
219 and Barrie, 1999), and Trapper Creek (Interagency Monitoring of Protected Visual Environments;
220 IMPROVE). It is noted that the measurements at Trapper Creek only include dust particles smaller
221 than $2.5 \mu m$ and are only compared with simulated dust concentrations at the same size range. All
222 other concentration measurements capture dust particles below $40 \mu m$ and are compared with
223 simulated dust over the whole size range ($< 10 \mu m$). The dust deposition fluxes dataset, which
224 including 84 stations, is also the same as Huneus et al. (2011). The locations of the observation
225 network are shown in Figure 2d, with the AOD data taken close to source regions and the dust
226 surface concentrations and deposition fluxes measured at relatively remote regions. The Pearson
227 correlation coefficient (r) are provided for each comparison. We note that the comparisons are
228 subject to representative biases caused by comparing an observational station with a global model
229 grid point (with a horizontal resolution of ~ 100 km). The comparisons of dust concentration and

Deleted: Aerosol Robotic

Deleted: Fan, 2013

232 deposition flux also have systematic errors because the measurements were for a different time
233 period than that of the model simulation.

234 In general, the three comparisons indicate that our CTRL simulation is capable of capturing the
235 global dust cycle in both near the source and remote regions. As shown in Figure 2a, the modeled
236 AOD is within a factor of two of the observations over most of the stations. The correlation of the
237 AOD comparison is 0.73, which is comparable to the best performing simulation ($r = 0.72$) in Kok
238 et al. (2014b). Our model also does a fairly good job in simulating the dust surface concentrations
239 (Figure 2b) and produces a correlation coefficient of 0.84. For the three high latitude sites, the
240 model shows moderate underestimation at Heimaey and Trapper Creek, and large positive bias at
241 Alert (see discussion below). The correlation coefficient for simulated dust deposition fluxes ($r =$
242 0.48) is also within the range of the AeroCom comparisons (0.08 to 0.84) in Huneus et al. (2011).
243 The model results over most of the sites are within one order of magnitude difference, except at
244 the polar regions. In particular, the model overestimates the dust deposition flux in Greenland (red
245 triangles in Figure 2c and 2d) by around two orders of magnitude, likely due to too strong local
246 emissions simulated near the coast of Greenland (Figure 1a).

247 The seasonal cycle of dust surface concentrations at the three Arctic stations (Heimaey, Alert,
248 and Trapper Creek) are shown in Figure 3, along with the contribution from seven tagged sources.
249 The simulated dust concentrations at Heimaey are dominated by HLD and agree well with the
250 observation in late summer and autumn (Figure 3a). Its annual-averaged low bias shown in Figure
251 2b mainly comes from the springtime, when Prospero et al. (2012) found the observed dust are
252 related to dust storms in Iceland, indicating a possible underestimation in the simulated Icelandic
253 dust during this time. The HLD also dominates the surface dust concentrations at Alert (Figure 3b),
254 leading to a Jarge overestimation from June to August in our simulation, which possibly implies a

Deleted: 83

Deleted: , but

Deleted: significant

Deleted: September

259 high bias and wrong seasonal cycle of HLD emission over Greenland and North Canada. The
260 Trapper Creek station is instead dominated by LLD from East Asia and shows an underestimation
261 for most of the year. It is noted that we only include fine dust (diameter < 2.5 μm) for the
262 comparison at Trapper Creek. Larger size range is likely to be more influenced by HLD sources.
263 The low bias here, especially that during the autumn, can be related to the missing of local
264 emissions from the coast of Southern Alaska (Figure 1a) that occurs most frequently in autumn
265 (Crusius et al., 2011). An underestimation of the transport from Saharan dust may also contribute
266 slightly, as the influence from Saharan dust is found during mid-May at Trapper Creek (Breider et
267 al., 2014).

268 The simulated Arctic dust vertical profiles are also compared with the measured dust
269 concentrations during the Arctic Research of the Composition of the Troposphere from Aircraft
270 and Satellites (ARCTAS) flight campaign (Figure 4) (Jacob et al., 2010). The ARCTAS campaign
271 was conducted over the North American Arctic in April and July 2008. The simulated profiles are
272 averaged over the regions where the aircraft flew, in accordance with Groot Zwaafink et al. (2016).
273 In April, the model does a good job in capturing the Arctic dust vertical profiles (Figure 4a).
274 However, in July, the model underestimates dust by a factor of 2 to 5 between 3 and 10 km (Figure
275 4b). It also shows an overestimation near the surface in July, which agrees with the surface
276 concentrations comparison at Alert station (Figure 3b). The underestimation in the upper
277 troposphere and overestimation near the surface likely imply a too weak vertical transport of HLD
278 in the North American Arctic in summertime. The high bias in the upper troposphere may also be
279 related to an underrepresentation of LLD transport.

280 Finally, we evaluate the simulated dust extinction against the Cloud-Aerosol Lidar and Infrared
281 Pathfinder Satellite Observation (CALIPSO) retrieval (Luo et al., 2015a, b), which includes

Deleted: 2015b, a

283 nighttime dust extinction for the period of 2007 to 2009. The Luo et al. (2015a, b) data set has
284 improvements in dust separation from other aerosol types and thin dust layer detection in the Arctic
285 than the standard CALIPSO product (Winker et al., 2013). To make an apple-to-apple comparison,
286 the modeled dust extinction is sampled along the CALIPSO tracks and screened by cloud fraction
287 (Wu et al., 2020). For this comparison, we only use the first three years (2007 to 2009) of the
288 CTRL simulation to be consistent with the observation period. Overall, the model does a good job
289 in capturing the Arctic dust extinction vertical profiles (Figure 5). We notice that the simulated
290 dust extinction is lower than CALIPSO retrievals at the upper troposphere in summer, which
291 agrees with the ARCTAS comparisons. The simulated dust extinction also shows a consistent
292 underestimation in springtime (MAM) and a near surface underestimation in wintertime (MAM).
293 Since the Arctic is mostly covered by ice and snow in these two seasons, the impacts of HLD are
294 expected to be limited and the low biases are most likely due to the underprediction of LLD
295 transport. The near surface underestimation in DJF may indicate a too weak LLD transport in the
296 lower troposphere (e.g., the transport of dust emitted from Central Asia; see Figure 7 and the
297 corresponding discussions in Section 3.2). Moreover, the HLD has a large contribution in the lower
298 troposphere in boreal summer and autumn, which is consistent with its strong emission at that time.
299 In contrast, LLD plays a more dominant role in the upper troposphere, where African dust
300 contributes the most in the springtime and East Asian dust has a larger contribution in the other
301 seasons.

302 3.2 Arctic dust mass source attribution

303 Table 2 summarizes the relative contributions from individual sources to the total Arctic dust
304 burden. The transport pathways can be identified from the dust burden spatial distribution for each
305 source in Figure 6, while the relative contribution of each source to the total dust burden is shown

Deleted: , while the

Deleted: .

308 [in Figure S2](#). We also calculate the regional burden efficiency for each source (Table S1), which
309 is defined as the mean contribution to the Arctic dust column burden divided by the corresponding
310 dust emission (H. Wang et al., 2014). This metric represents the sensitivity of Arctic dust loading
311 to per unit change of dust emission from each source (i.e., the poleward transport efficiency of
312 each source).

313 Our model results suggest that the HLD (Arc) is the largest contributor (30.7%) to the annual
314 mean Arctic dust burden among all the tagged sources. As shown in Figure 6a [and Figure S2a](#), the
315 local dust is confined within the high latitudes, with the higher amounts [and higher contributions](#)
316 [to the total dust burden](#) near the sources in North Canada, coast of Greenland, and Iceland. The
317 interior of the Greenland ice sheet, with its higher elevations, is more influenced by LLD from
318 ~~North Africa and East Asia than HLD, (Figure S2c and S2f). This is due to the weak vertical~~
319 ~~transport of local emissions in the Arctic (see more discussions below).~~

320 On the other hand, all LLD sources are responsible for 69.3% of the dust loading in the Arctic,
321 with considerable contributions from North Africa (24.2%) and Asia (in total 44.2%; EAs: 19.9%,
322 MSA: 11.5%, CAs: 12.8%), and minor contributions from NAM (0.1%) and RoW (nearly 0). The
323 North African dust is primarily transported westward to the Atlantic and southward to Sahel, with
324 a smaller fraction transported directly northward or northeastward across the Eurasia to the Arctic
325 (Figure 6c; Shao et al., 2011). The westward trajectory can also bring dust to the Arctic through
326 the Azores high (e.g., VauCuren et al., 2012), but this pathway is not clearly seen on Figure 6c
327 likely due to the strong wet removal process over the North Atlantic. As evident by the low
328 transport efficiency in Table S1, the significant contribution of the North African dust to the Arctic
329 dust burden is mainly due to its massive emission. However, this is not the case for EAs. The East
330 Asian dust is first lifted vertically by topography and convection (Shao et al., 2011) and is widely

- Deleted:** Asia and
- Deleted:** .
- Deleted:** suppression of
- Deleted:** by the stratified atmosphere as well as limited convection
- Deleted:** Baddock et al., 2017; Bullard et al., 2016).

336 spread over the Northern Hemisphere mid- and high-latitude regions through the westerly flow in
337 the upper troposphere (Figure 6f). The high elevation of East Asian dust plumes results in weaker
338 removal processes and thus an efficient poleward transport. As shown in Table S1, the annual
339 transport efficiency of the East Asian dust is relatively high among the LLD sources, which is
340 nearly three times larger than that of the North African dust. The poleward transport of dust from
341 CAs and MSA both takes the pathway across Siberia (Figure 6d and 6e). The transport efficiency
342 of the CAs dust is two times higher than that of the MSA dust (Table S1). This is attributed to CAs
343 being closer to the Arctic and having less southward dust transport than MSA. Overall, the LLD
344 from North Africa and Asia contributes more to the Eurasia and Pacific sector of the Arctic
345 (Figures S2e to S2f). The impact of NAM dust is limited by its weak emission (Figure 6b), while
346 dust emitted in the Southern Hemisphere (RoW) can hardly pass the equator (Figure 6g).

347 Earlier modeling studies (Breider et al., 2014; Groot Zwaafink et al., 2016; Luo et al., 2003;
348 Tanaka and Chiba, 2006) also quantify the relative contributions of dust from various regions to
349 the Arctic dust loading. Among these studies, only Groot Zwaafink et al. (2016) includes HLD.
350 Our estimate about the HLD percent contribution is close to that from their study (27%). For LLD,
351 our conclusion about the dominant role of African and Asian dust to the Arctic dust burden is also
352 corroborated by these previous studies. However, the relative importance of African and Asian
353 dust is uncertain. Based on our results, the Asian dust is responsible for 65% of the LLD transport
354 to the Arctic, while the African dust only contributes 35%. Other studies find that 50% (Groot
355 Zwaafink et al., 2016; Luo et al., 2003; Tanaka and Chiba, 2006) to as much as 65% (Breider et
356 al., 2014) of the LLD in the Arctic is attributed to North Africa. These discrepancies may be
357 explained by the different dust emission and scavenging, dust size distribution, meteorological
358 fields, and/or time periods for the model simulation. For example, North Africa dust in our study

359 contributes slightly less (51.9%) to the global dust emission than the other studies (from 57% to
360 67%). Isotopic analysis (Bory et al., 2002, 2003) and case studies (Huang et al., 2015; Stone et al.,
361 2005; VanCuren et al., 2012) have proved that both Asian and African dust can be transported to
362 the Arctic. However, it remains unclear which of them contributes more to the Arctic dust loading
363 due to the limited observational constraints.

364 HLD and LLD source regions also have very distinct vertical distributions in the Arctic. Figures
365 7a and 7b show the annual mean vertical profiles of Arctic dust concentrations from various
366 sources and their percentage contributions, respectively. The Arctic dust in the lower atmosphere
367 is dominated by the local source. HLD accounts for more than 30% of the Arctic dust

368 concentrations below 800 hPa, with up to 85% contribution near the surface. ~~However, the HLD~~
369 ~~contribution decreases rapidly with height and is less than 10% above 700 hPa. This is because the~~
370 ~~lower troposphere of the Arctic is more stratified than the mid- and low latitudes, which suppresses~~
371 ~~the vertical transport of HLD. The lower tropospheric stability (LTS) from the CTRL simulation~~
372 ~~and comparison with the MERRA2 reanalysis data are shown in Figure S3. The weak HLD vertical~~
373 ~~transport in the Arctic is also reported by previous studies (Groot Zwaafink et al., 2016, Baddock~~
374 ~~et al., 2017; Bullard, 2017). Moreover, the LTS over the Arctic sea ice is much larger than that~~
375 ~~over open ocean surface (Schweiger et al., 2008), which may lead to a stronger vertical transport~~
376 ~~of HLD over open waters. This suggests that the vertical transport of HLD may change with the~~
377 ~~sea ice reduction in a warming future.~~

378 In contrast, LLD has a higher contribution in the mid- and upper troposphere than near the
379 surface. Such a vertical distribution of LLD is consistent with Stohl (2006) and Groot Zwaafink
380 et al. (2016). As Stohl (2006) found, aerosols originating from the warm subtropics are transported
381 poleward following the uplifted isentropes and the Arctic lower atmosphere is dominated by the

Deleted: However, due to the weak vertical transport, the HLD contribution decreases rapidly with height and is less than 10% above 700 hPa.

385 near-impenetrable cold polar dome. Therefore, there is a slantwise lifting of low latitude aerosols
386 during their poleward transport. NAF and EAs are the two key contributors to the Arctic dust
387 vertical concentrations, each of which contributes up to one third of the total dust concentrations
388 above 700 hPa. Dust emission from MSA also has a moderate contribution (15-20%) that increases
389 gradually with height, while the contribution from CAs peaks at 700 to 800 hPa, indicating a lower
390 altitude transport pathway than the EAs and MSA dust.

391 In addition, the Arctic dust undergoes a strong seasonal cycle (Table 2 and [Figures 7c-j](#)).
392 Because of the strong local emissions (Figure 1c), about half of the Arctic dust burden in summer
393 and autumn come from HLD, with more than 50% contribution of Arctic dust concentrations
394 below 850 hPa in these two seasons. In contrast, LLD plays a dominant role in spring and winter.
395 The North African dust has the largest contribution in spring, which accounts for about 45% of the
396 total dust concentrations above 700 hPa. The East Asian dust is more important in the other three
397 seasons. Due to its high emission height, the relative contribution from EAs tends to increase with
398 height and reaches 30% to 50% of the total dust concentration above 500 hPa in summer, spring,
399 and winter.

400 3.3 Immersion freezing on dust in the AMPCs

401 We are particularly interested in the contribution of various dust sources to the Arctic INP
402 populations. Therefore, we compare the simulated INP concentrations with nine Arctic field
403 measurements, which are summarized in Table 3. The modeled dust INP concentrations are
404 diagnosed from monthly averaged aerosol properties using [the default CNT scheme and two](#)
405 [empirical](#) ice nucleation parameterizations, DeMott et al. (2015; hereafter as D15) and Sanchez-
406 Marroquin et al. (2020; hereafter as SM20). The D15 parameterization, which is [representative of](#)
407 Saharan and Asian [desert](#) dust, relates dust INP number concentrations to the number

Deleted: Figure

Deleted: two

Deleted: derived for the

411 concentration of dust particles larger than 0.5 μm diameter and is found to produce the most
412 reasonable LLD INP concentrations in EAMv1 (Shi and Liu, 2019). ~~CNT and D15 are~~ applied to
413 LLD only and all the dust aerosols (LLD and HLD) in ~~Figures 8a-b and Figures 8d-e~~, respectively.
414 The SM20 parameterization, which is derived for the HLD Icelandic dust, describes the dust INP
415 number concentrations as a function of surface active site density and total dust surface area.
416 Considering the possibly different ice nucleation ability between HLD and LLD, we only applied
417 the SM20 parameterization to HLD and the ~~CNT and D15 parameterizations are~~ still applied to
418 LLD in ~~Figures 8c and 8f, respectively~~. To account for the contributions from other aerosol types,
419 we also calculate the INP concentrations from BC (Fig. ~~8g~~) and sea spray aerosol (SSA; includes
420 MOA and sea salt) (Fig. ~~8h~~) following Schill et al. (2020; hereafter as Sc20) and McCluskey et al.
421 (2018; hereafter as M18), respectively. ~~More details about the ice nucleation parameterizations are~~
422 ~~provided in Text S2. We discuss the choice of dust ice nucleation schemes in Text S2.6 in the~~
423 ~~Supplement.~~
424 Overall, only including LLD as INPs results in up to four orders of magnitude underprediction
425 compared to observations (~~Figures 8a and 8d~~), while taking into account the contribution from
426 HLD greatly improves the model performance by increasing the simulated dust INP concentrations
427 (~~Figures 8b, 8c, 8e, and 8f~~). ~~The CNT parameterization produces 5 to 10 times more INP~~
428 ~~concentrations than the other two schemes at moderately cold temperatures (-22 to -28°C), while~~
429 ~~it has a significant underestimation of observed INP concentrations at warm temperatures ($T > -$~~
430 ~~18°C) (also see Figure S4). D15 and SM20 agree well with each other in simulating HLD INPs,~~
431 with SM20 producing slightly higher results than D15. Our modeling results also indicate that BC
432 and SSA have much less contributions to INP than dust in all the nine field campaigns (Figure ~~8g~~
433 and ~~8h~~).

Deleted: It is

Deleted: Figure

Deleted: Figure 8b

Deleted: parameterization is

Deleted: Figure

Deleted: 8d

Deleted: 8e

Deleted: Figure

Deleted: Figure 8b and 8c). The two dust parameterizations

Deleted: 8d

Deleted: 8e

445 A detailed analysis of sources of the INPs for the nine datasets based on modeling analyses and
446 the corresponding observations in the literature are provided in Table 3. Modeling results indicate
447 that HLD has larger contributions to the INPs for the campaigns conducted in summer and autumn
448 than spring, in agreement with the observations. Also, ground-based measurements are more
449 influenced by the nearby HLD sources, while LLD from EAs and NAF contributes more to the
450 aircraft measurements.

451 Our modeling analyses about the INP sources agree well with the observational studies at Alert
452 in spring 2016 and near Iceland in autumn 2014 (symbol “C” and “I” in Figure 8, respectively),
453 while the model underestimates the observed INP concentrations in both cases. The low bias in
454 dataset C indicates an underprediction in the long-range transport of Asian dust to the Arctic
455 surface in springtime. The underestimation in dataset I is more likely due to the fact that some of
456 the aircraft measurements were taken inside the Icelandic dust plumes (Sanchez-Marroquin et al.,
457 2020), which cannot be resolved by the monthly mean model output and the coarse model
458 horizontal resolution (1°). Such uncertainties exist in all the model-observation comparisons.

459 Some other comparisons in INP sources reveal the lack of marine and carbonaceous INPs in the
460 model. The model results show a dominance of dust INPs in spring 2017 at Zeppelin and Oliktok
461 Point (symbol “D” and “E” in Figure 8) and in Autumn 2004 at Utqiagvik (symbol “H” in Figure
462 8), while the observational studies suggested the importance of marine sources at the first two
463 locations and of carbonaceous aerosols at Utqiagvik. Therefore, it is likely that the model
464 underestimates the contribution of MOA (Wilson et al., 2015; Zhao et al., 2021a) and does not
465 account for terrestrial biogenic INPs (Creamean et al., 2020) due to the lack of treatments in the
466 model. In addition, both D15 and SM20 schemes cannot represent the high ice nucleating ability
467 of HLD at warm temperatures at Zeppelin in summer 2016 (symbol “G” in Figure 8), which is

468 attributed to soil organic matter by Tobo et al. (2019). When these organics are taken into account
469 in the model, model overestimation for site G will get even worse, implying an overestimation of
470 surface dust concentrations and/or HLD dust emission at Svalbard in the summertime. In summary,
471 the model's INP biases in the Arctic are likely due to biases in the simulated aerosol fields (e.g.,
472 dust, MOA, and BC) and uncertainties in current ice nucleation parameterizations or missing
473 representations of other INP sources (e.g., terrestrial biogenic aerosols).

474 In addition, it is noted that we do not explicitly represent the potential ice nucleation ability
475 differences in freshly emitted HLD and long-range transported LLD caused by the chemical aging
476 and coating of dust (Boose et al., 2016). However, D15 and SM20 may already take the aging
477 effect into account implicitly. Because D15 includes Saharan and Asian dust data collected over
478 Pacific Ocean basin and US Virgin Islands, respectively, which are far away from the
479 corresponding LLD sources, while SM20 are derived from freshly emitted Icelandic dust, which
480 is subjected to less aging processes.

481 The comparisons above are based on INP concentrations at a given temperature set by the INP
482 instruments, which reflects the potential INP populations under ambient aerosol conditions. Next,
483 we examine the immersion freezing rate of dust originating from the seven tagged sources (Figure
484 9) to evaluate the influences of HLD and LLD on ice nucleation processes in mixed-phase clouds.
485 It is noted that the immersion freezing rate here is calculated online in the model using the ambient
486 temperature and the default CNT ice nucleation parameterization.

487 Compared with its contribution to the dust burdens, the contribution of the HLD to the annual
488 mean mixed-phase cloud immersion freezing rate is relatively small (~10% below 600 hPa)
489 (Figure 9a). This is because the HLD is mainly located in the lower troposphere and not a lot of
490 HLD can reach the mixed-phase cloud levels (or the freezing level), especially under the case that

491 the HLD tends to be more prevalent in the warm seasons (see more discussion below). Among the
492 LLD sources, North African dust (Figure 9c) and East Asian dust (Figure 9f) are the two major
493 contributors, both of which are responsible for more than 20% of the annual mean immersion
494 freezing rate in the mixed-phase clouds. Consistent with the vertical distribution of dust
495 concentrations, the North African dust has its maximum contribution (30-40%) at around 500 hPa,
496 while the East Asian dust plays a more important role at higher altitudes (above 400 hPa). Dust
497 from Central Asia also has a moderate contribution (~20%) to the immersion freezing rate in the
498 Arctic (Figure 9d).

499 Considering the different seasonality of HLD and LLD in the Arctic, we next investigate the
500 seasonal variations of the immersion freezing rate in the Arctic mixed-phase clouds from HLD
501 and two dominating LLD sources (NAf and EAs) (Figure 10). HLD has the largest contribution to
502 the Arctic immersion freezing rate in boreal autumn, with more than 30% below 700 hPa and up
503 to 50% near the surface (Figure 10c). It is related to the prevalence of HLD and relatively cold
504 temperatures during this time in the Arctic. This is not the case for the summer, when the freezing
505 level is relatively high. Although it is responsible for 50% of the total Arctic dust burden in the
506 boreal summer, HLD has a limited contribution to the immersion freezing rate in the clouds (Figure
507 10b), because its weak vertical transport makes it hard to reach the freezing line. The contrast
508 results in summer and autumn suggest that the immersion freezing rate in the Arctic clouds is
509 influenced by air temperature in addition to the aerosols. It also implies that the surface INP
510 measurements may not reflect the complete picture of INP effects and more aircraft INP
511 measurements are needed in the future. The seasonal variations of the immersion freezing rate
512 from NAf and EAs are weaker than that from HLD, but are still subjected to the vertical temperature

Deleted: .

514 change with season. The North African dust contributes more in spring and winter, while the East
515 Asian dust is more important in summer and autumn.

516 **3.4 Impact on cloud properties and radiative fluxes**

517 Dust INPs can freeze the supercooled liquid droplets, which impacts the cloud microphysical
518 and macrophysical properties and modulates the Earth's radiative balance. To examine such
519 impacts, we conduct three sensitivity experiments that turn off the heterogeneous ice nucleation in
520 the mixed-phase clouds by dust from Arctic local source, North Africa, and East Asia, respectively
521 (i.e., noArc, noNAf, and noEAs in Table 1). The impacts of dust INPs from each source are
522 determined by subtracting the respective sensitivity experiment from CTRL. Due to the feedbacks
523 in dust emission and wet scavenging caused by changing cloud properties, the dust concentrations
524 in the sensitivity experiments are not identical to CTRL, but the absolute differences are mostly
525 within 5% (Figure S5 in the Supplement).

526 The cloud liquid and ice changes caused by dust INPs from each source are shown in Figure 11.
527 Due to the strengthening of heterogeneous ice nucleation processes, INPs from all the three sources
528 consistently reduce the total liquid mass mixing ratio (TLIQ) (Figure 11, first column) and cloud
529 liquid droplet number concentration (NUMLIQ) (Figure 11, third column). The influence of HLD
530 is mainly in the lower troposphere (Fig. 11, top row) and the influence of LLD extends to higher
531 altitudes (Fig. 11, bottom two rows). Moreover, the cloud ice number concentration (NUMICE)
532 decreases in the upper troposphere (Figure 11, fourth column), likely due to less cloud droplets
533 available for the homogeneous freezing in cirrus cloud after introducing dust INPs in the mixed-
534 phase clouds. With fewer ice crystals falling from the cirrus clouds to the mixed-phase clouds, the
535 WBF process in the mixed-phase clouds is inhibited (Figure S6). Other ice phase processes such
536 as the accretion of cloud water by snow and the growth of ice crystals by vapor deposition also

Deleted: S2

Deleted: supporting information

Deleted: S3

540 become less efficient, which decreases the total ice mass mixing ratio (TICE) above 600-700 hPa
541 altitude (Figure 11, second column). TICE in the lower troposphere is increased because of
542 immersion freezing and snow sedimentation from above.

543 Since liquid water path (LWP) is found to play a critical role in the Arctic radiative budget (e.g.,
544 Dong et al., 2010; Hofer et al., 2019; Shupe and Intrieri, 2004), we further investigate the seasonal
545 variations of LWP changes caused by dust INPs from the three sources (Figure 12). Corroborated
546 with their large contribution to the immersion freezing rate during this time (Figure 10, top row),
547 HLD INPs produce the strongest LWP decrease (-1.3 g m^{-2}) in boreal autumn (Figure 12c),
548 especially over North Canada and Greenland. The influence of LLD INPs on LWP peaks in spring
549 and winter. North African dust tends to have a larger impact on North Eurasia, while East Asian
550 dust impacts the west Arctic more.

551 Dust INPs from the three sources consistently increase (decrease) the annual mean downwelling
552 shortwave (longwave) radiative flux (FSDS and FLDS) at the surface (Figure 13, left and middle
553 columns). This is mainly due to the LWP decrease, which reduces the cloud albedo and longwave
554 cloud emissivity. For HLD INPs, the FLDS reduction dominates over the FSDS increase and
555 causes a net cooling effect at the Arctic surface (-0.24 W m^{-2}) (Figure 13c). In contrast, FSDS and
556 FLDS changes related to the LLD INPs are comparable, which cancels each other and yields a
557 small net radiative effect (0.08 W m^{-2} for NAF and -0.06 W m^{-2} for EAs) (Figure 13, bottom two
558 rows). These differences in the net radiative effect are associated with different seasonalities of
559 HLD and LLD. The insolation in the Arctic is strong in spring and summer but very limited in
560 autumn and winter. Since the HLD INPs have much stronger influence on LWP in autumn and
561 winter than spring and summer (Figure 12), their contribution to the FSDS warming is weak and
562 the FLDS cooling in autumn and winter dominates the annual mean effect (Table 4, part 1; also

563 seen in Figure [S7](#) to [S9](#)). LLD INPs are also important in spring and summer, so their FS
564 DS warming effect is comparable to, and compensates for, the FLDS cooling effect.

Deleted: S4

Deleted: S6

565 We also examined the dust INP effect on cloud radiative forcing (CRF) at the top of the
566 atmosphere (TOA) (Table 4, part 2). Dust INPs from the three sources induce a small net cooling
567 (from -0.03 to -0.05 W m⁻²) in the Arctic, with SW warming and LW cooling effects. The net
568 cooling persists throughout the year, except for the summertime when the sufficient insolation
569 results in a strong SW warming and, consequently, a net warming effect. Shi and Liu (2019) also
570 found LLD can induce a generally net cooling effect above 70°N (0.18 to -1.95 W m⁻²), but in a
571 much higher magnitude than the sum of NAF and EAs dust INP effects (-0.15 W m⁻² above 70°N,
572 not shown in Table 4), which implies the aerosol glaciation effect on mixed-phase clouds is highly
573 non-linear.

574 Finally, we evaluate the model performance in simulating the Arctic LWP and radiative fluxes
575 against the Moderate Resolution Imaging Spectroradiometer (MODIS) LWP (Platnick et al., 2003)
576 and the Cloud and the Earth's Radiant Energy System Energy Balanced and Filled Edition 4.1
577 (CERES-EBAF Ed4.1) products (Loeb et al., 2018; Kato et al., 2018), respectively (Figure 14).
578 Two MODIS datasets are used, including the standard product (Platnick et al., 2003; P03) and an
579 improved one (Khanal et al., 2020; K20) that corrected the positive bias in the Arctic in P03. The
580 MODIS simulator is used for the LWP comparison. According to Fig. 14, the simulated LWP from
581 the four experiments are lower than P03 but higher than K20. All the four experiments also
582 underestimate FS
583 DS with too strong SWCF and overestimate FLDS with too strong LWCF, which
584 likely points to the biases of modeled clouds (e.g., too much LWP as compared to K20). The
585 differences among the model experiments are very small compared to their discrepancies with
observations. We notice including dust INPs from the three sources decreases the simulated LWP

588 (i.e., CTRL has less LWP than the other experiments) (Figure 14a), which makes the model
589 performance better if compared to K20. Moreover, it shows noticeable improvements in simulating
590 both surface and TOA radiative fluxes after including dust INPs from each of the three sources
591 (i.e., the results from CTRL are closer to the CERES results than the other three experiments)
592 (Figure 14b-e).

593 Overall, including HLD or LLD INPs do not contribute a lot to the reduction of biases in
594 simulating the LWP and radiative fluxes in the AMPCs. However, the representation of AMPCs
595 in global climate models is associated with multiple cloud macro- and microphysical processes,
596 and large-scale dynamics (Morrison et al., 2012) (see more discussion in Section 4), which interact
597 with one another non-linearly. Therefore, even though including HLD or LLD INPs do not
598 improve the representation of AMPCs significantly in our model, a good representation of dust
599 INPs, especially including HLD INPs, could still be of great importance for parameterizing
600 AMPCs in the model.

601 **4. Discussion**

602 The HLD emission in our CTRL simulation is manually tuned up by 10 times to match the
603 estimate by Bullard et al. (2016), which is derived by compiling field measurements in Iceland and
604 Alaska. Since the instruments were operated under extreme Arctic conditions and the sampling is
605 very scarce, this estimate may have large uncertainties. Therefore, the tuned HLD emission can be
606 biased as well. Considering the overestimation of Greenland dust deposition, summertime surface
607 dust concentrations at Alert station, and surface INP concentrations at Svalbard, our tuning may
608 cause a regional and temporal high bias in HLD dust emissions. We examine this uncertainty by
609 conducting a sensitivity experiment with halving HLD emissions in CTRL (i.e., HLD_half) and

610 analysing the interannual variability of CTRL and HLD_half simulations (Table S2 and [Figures](#)
611 [S10-S11](#)). The HLD_half simulation indeed has a better performance than CTRL. However, the
612 high bias for Greenland deposition and the summertime overestimation of Alert dust surface
613 concentration still exist, which reflects the limitation of the dust emission parameterization we use.
614 This parameterization may not be able to capture the spatial distribution of dust emissions across
615 the Arctic, considering that the model performance at other sites (e.g., Heimaey, Figure 3a) is
616 much better. Also, the HLD emissions and their regional distributions have large interannual
617 variabilities. Therefore, [as we mentioned in Section 3.1](#), comparing model simulations with
618 measurements conducted in different years may result in large uncertainties.

619 The overestimation of surface dust and INP concentrations may imply a too weak vertical
620 transport of HLD, considering the low biases of dust in the upper troposphere as compared with
621 ARCTAS measurements and CALIPSO retrievals. The weak vertical transport at the source
622 regions in EAMv1 was also found in Wu et al. (2020), which was related to the too strong dry
623 deposition at the surface layer. If this bias is addressed, HLD would contribute less (more) to the
624 Arctic dust concentrations in the lower (upper) troposphere, which suggests a larger contribution
625 of HLD to the heterogeneous ice nucleation in the mixed-phase clouds in the summertime. As a
626 result, the HLD would induce a more positive net downwelling radiative flux at the surface in
627 summer and a less negative annual mean radiative effect. It is also noted that the underprediction
628 in the upper troposphere dust may come from a weak long-range transport of LLD. If this is the
629 case, the HLD would have a weaker contribution to the upper level dust concentrations and likely
630 less of an impact on mixed-phase cloud heterogeneous ice nucleation in the summertime.

631 In addition, EAMv1 has intrinsic biases in its cloud microphysics parameterizations. As
632 mentioned in Section 2.1, the WBF process rate in EAMv1 is tuned down by a factor of 10, which

Deleted: Figure S7-S8

634 results in too many supercooled liquid clouds in high latitudes (Y. Zhang et al., 2019; M. Zhang
635 et al., 2020). Shi and Liu (2019) found the sign and magnitude of dust INP cloud radiative effect
636 in the Arctic would change, after removing the tuning factor for the WBF process in EAMv1.
637 Moreover, EAMv1 does not account for several secondary ice production mechanisms, which are
638 suggested to have a large impact on the ice crystal number concentrations and thus cloud phase
639 (Zhao and Liu, 2021; Zhao et al., 2021b). All these uncertainties in the cloud microphysical
640 processes would interact non-linearly and influence our estimate of INP radiative effect and should
641 be addressed in future studies.

642 **5. Conclusions**

643 In this study, we investigate the source attribution of dust aerosols in the Arctic and quantify the
644 relative importance of Arctic local dust versus long-range transported LLD to the Arctic dust
645 loading and INP population. We found that HLD is responsible for 30.7% of the total dust burden
646 in the Arctic, whereas LLD from Asia and North Africa contributes 44.2% and 24.2%, respectively.
647 The vertical transport of HLD is limited due to the stable cold air in the Arctic and thus it
648 contributes more to the dust burden in the lower troposphere. In boreal summer and autumn when
649 the contribution of HLD is at a maximum because of stronger local dust emissions, HLD is
650 responsible for more than 30% of the Arctic dust loading below 800 hPa, but less than 10% above
651 700 hPa. In contrast, LLD from North African and East Asian dust dominates the dust burden in
652 the free troposphere, since the poleward transport of LLD follows the uplifted isentropes. The
653 North African and East Asian dust accounts for about two thirds of the dust loading above 700
654 hPa, with the remaining one third from other LLD sources. The North African dust contributes
655 more between 500 and 700 hPa, while the East Asian dust dominates in the upper troposphere

656 (above 400 hPa) because of its high emission heights. In addition, the North Africa source has a
657 larger contribution in springtime, while the other three seasons are more influenced by the East
658 Asian source.

659 Modeled dust INP concentrations are investigated following two ice nucleation
660 parameterizations: D15 and SM20. Compared with INP measurements, our results show that
661 including HLD as INPs significantly improves the model performance in simulating Arctic INP
662 concentrations, especially for the ground measurements and for the measurements conducted in
663 summer and autumn. We also examine the INP contributions from BC and SSA based on Sc20
664 and M18, respectively. The model suggests that both of them are only weak sources compared
665 with dust. We note that the model may underestimate SSA INPs and currently misses the
666 representation of terrestrial biological INPs. The model biases of INPs can also be due to bias in
667 simulating Arctic dust concentrations and/or the uncertainties in ice nucleation parameterizations.

668 We examine the contribution of dust from the three sources (Arctic, North Africa, and East Asia)
669 to the ambient immersion freezing rate in the Arctic. The contribution from HLD shows a strong
670 seasonal variation, with the peak contribution in boreal autumn (above 20% below 500 hPa). In
671 summer, although HLD has strong contributions to the dust loading and INP concentrations in the
672 lower troposphere, its impact on the ambient immersion freezing rate is limited due to the warm
673 temperatures and weak vertical transport. This finding implies that surface INP measurements may
674 not be sufficient in representing the INP population in the Arctic mixed-phase clouds and more
675 measurements of INP vertical profiles are needed in the future. North African and East Asian dust
676 are the two major LLD contributors to the ambient immersion freezing rate. The annual mean
677 contribution (30-40%) from North African dust peaks at around 500 hPa, while the immersion

678 freezing is dominated by East Asian dust (more than 40%) in the upper troposphere (above 400
679 hPa).

680 The cloud glaciation effect of dust INPs from local Arctic sources, and North African and East
681 Asian sources, is further examined. It is found that INPs from all the three sources consistently
682 result in a reduction in TLIQ and NUMLIQ. TICE and NUMICE at higher altitude also decrease,
683 likely due to the weakening of homogeneous freezing in cirrus clouds. LWP reduction caused by
684 HLD INPs is evident in autumn and winter, while those by dust INPs from the two LLD sources
685 peak in spring. HLD INPs also drive a net cooling effect of -0.24 W m^{-2} in the downwelling
686 radiative flux at the surface in the Arctic, while the net radiative effects of the two LLD INP sources
687 are relatively small (0.08 W m^{-2} for NAF and -0.06 W m^{-2} for EAs). This variation in radiative
688 effect reflects the seasonal difference between HLD and LLD. Our results also suggest that all the
689 three dust sources result in a weak negative net cloud radiative effect (-0.03 to -0.05 W m^{-2}) in the
690 Arctic, which is consistent with Shi and Liu (2019).

691 Overall, our study shows that the Arctic local dust, which has been overlooked in previous
692 studies, may have large contributions to the Arctic dust loading and INP population. It can also
693 influence the Arctic mixed-phase cloud properties by acting as INPs. Considering the climate
694 impacts of local Arctic dust emissions will be important given a warming climate, where reduction
695 in snow coverage and more exposure of dryland in the Arctic may lead to increased HLD emissions.

696 *Code availability.* The E3SM code is available on GitHub: [https://github.com/E3SM-
697 Project/E3SM.git](https://github.com/E3SM-Project/E3SM.git).

698 *Author contribution.* YS and XL conceived the project. YS modified the code, conducted the
699 simulations, and led the analyses with suggestions from XL, MW, XZ, ZK, and HB. XL supervised

700 the study. YS wrote the first draft of the paper. All coauthors were involved in helpful discussions
701 and revised the paper.

702 *Competing interests.* The authors declare that they have no conflict of interest.

703 *Acknowledgements.* The authors would like to thank Drs. Meng Zhang and Sarah Brooks for their
704 comments and suggestions. Mingxuan Wu is supported by the US Department of Energy (DOE),
705 Office of Biological and Environmental Research, Earth and Environmental System Modeling
706 program as part of the Energy Exascale Earth System Model (E3SM) project. The Pacific
707 Northwest National Laboratory (PNNL) is operated for DOE by the Battelle Memorial Institute
708 under contract DE-AC05-76RLO1830. This research used resources of the National Energy
709 Research Scientific Computing Center, a DOE Office of Science User Facility supported by the
710 Office of Science of the U.S. Department of Energy under contract DE-AC02-05CH11231.

711 *Financial support.* This research was supported by the DOE Atmospheric System Research (ASR)
712 Program (grants DE-SC0020510 and DE-SC0021211).

713 **References**

714 Albani, S., Mahowald, N. M., Perry, A. T., Scanza, R. A., Zender, C. S., Heavens, N. G., Maggi,
715 V., Kok, J. F., and Otto-Bliesner, B. L.: Improved dust representation in the Community
716 Atmosphere Model, *J. Adv. Model. Earth Syst.*, 6, 541–570,
717 <https://doi.org/10.1002/2013MS000279>, 2014.

718 Arimoto, R., Duce, R. A., Ray, B. J., Ellis Jr, W. G., Cullen, J. D., and Merrill, J. T.: Trace elements
719 in the atmosphere over the North Atlantic, *J. Geophys. Res. Atmos.*, 100(D1), 1199–1213,
720 <https://doi.org/10.1029/94JD02618>, 1995.

721 Arnalds, O., Dagsson-Waldhauserova, P., and Olafsson, H.: The Icelandic volcanic aeolian
722 environment: Processes and impacts — A review, *Aeolian Res.*, 20, 176–195,
723 <https://doi.org/10.1016/j.aeolia.2016.01.004>, 2016.

Deleted: Xi Zhao,

Deleted: .

Formatted: Font color: Text 1

726 Atkinson, J. D., Murray, B. J., Woodhouse, M. T., Whale, T. F., Baustian, K. J., Carslaw, K. S.,
727 Dobbie, S., O'Sullivan, D., and Malkin, T. L.: The importance of feldspar for ice nucleation by
728 mineral dust in mixed-phase clouds, *Nature*, 498, 355–358, <https://doi.org/10.1038/nature12278>,
729 2013.

730 Baddock, M. C., Mockford, T., Bullard, J. E., and Thorsteinsson, T.: Pathways of high-latitude
731 dust in the North Atlantic, *Earth Planet. Sci. Lett.*, 459, 170–182,
732 <https://doi.org/10.1016/j.epsl.2016.11.034>, 2017.

733 de Boer, G., Morrison, H., Shupe, M. D., and Hildner, R.: Evidence of liquid dependent ice
734 nucleation in high-latitude stratiform clouds from surface remote sensors, *Geophys. Res. Lett.*, 38,
735 L01803, <https://doi.org/10.1029/2010GL046016>, 2011.

736 Bogenschutz, P. A., Gettelman, A., Morrison, H., Larson, V. E., Craig, C., and Schanen, D. P.:
737 Higher-order turbulence closure and its impact on climate simulations in the community
738 atmosphere model, *J. Clim.*, 26, 9655–9676, <https://doi.org/10.1175/JCLI-D-13-00075.1>, 2013.

739 Bory, A. J.-M., Biscaye, P. E., Svensson, A., and Grousset, F. E.: Seasonal variability in the origin
740 of recent atmospheric mineral dust at NorthGRIP, Greenland, *Earth Planet. Sci. Lett.*, 196, 123–
741 134, [https://doi.org/10.1016/S0012-821X\(01\)00609-4](https://doi.org/10.1016/S0012-821X(01)00609-4), 2002.

742 Bory, A. J.-M., Biscaye, P. E., and Grousset, F. E.: Two distinct seasonal Asian source regions for
743 mineral dust deposited in Greenland (NorthGRIP), *Geophys. Res. Lett.*, 30,
744 <https://doi.org/10.1029/2002GL016446>, 2003.

745 Breider, T. J., Mickley, L. J., Jacob, D. J., Wang, Q., Fisher, J. A., Chang, R. Y.-W., and Alexander,
746 B.: Annual distributions and sources of Arctic aerosol components, aerosol optical depth, and
747 aerosol absorption, *J. Geophys. Res. Atmos.*, 119, 4107–4124,
748 <https://doi.org/10.1002/2013JD020996>, 2014.

749 Bullard, J. E.: The distribution and biogeochemical importance of high-latitude dust in the Arctic
750 and Southern Ocean-Antarctic regions, *J. Geophys. Res. Atmos.*, 122, 3098–3103,
751 <https://doi.org/10.1002/2016JD026363>, 2017.

752 Bullard, J. E. and Austin, M. J.: Dust generation on a proglacial floodplain, West Greenland,
753 *Aeolian Res.*, 3, 43–54, <https://doi.org/10.1016/j.aeolia.2011.01.002>, 2011.

754 Bullard, J. E., Baddock, M., Bradwell, T., Crusius, J., Darlington, E., Gaiero, D., Gassó, S.,
755 Gisladottir, G., Hodgkins, R., McCulloch, R., McKenna-Neuman, C., Mockford, T., Stewart, H.,
756 and Thorsteinsson, T.: High-latitude dust in the Earth system, *Rev. Geophys.*, 54, 447–485,
757 <https://doi.org/10.1002/2016RG000518>, 2016.

758 Creamean, J. M., Kirpes, R. M., Pratt, K. A., Spada, N. J., Maahn, M., de Boer, G., Schnell, R. C.,
759 and China, S.: Marine and terrestrial influences on ice nucleating particles during continuous
760 springtime measurements in an Arctic oilfield location, *Atmos. Chem. Phys.*, 18, 18023–18042,
761 <https://doi.org/10.5194/acp-18-18023-2018>, 2018.

762 Creamean, J. M., Hill, T. C. J., DeMott, P. J., Uetake, J., Kreidenweis, S., and Douglas, T. A.:
763 Thawing permafrost: an overlooked source of seeds for Arctic cloud formation, *Environ. Res.*
764 *Let.*, 15, 084022, <https://doi.org/10.1088/1748-9326/ab87d3>, 2020.

765 Crusius, J., Schroth, A. W., Gassó, S., Moy, C. M., Levy, R. C., and Gatica, M.: Glacial flour dust
766 storms in the Gulf of Alaska: Hydrologic and meteorological controls and their importance as a
767 source of bioavailable iron, *Geophys. Res. Lett.*, 38, L06602,
768 <https://doi.org/10.1029/2010GL046573>, 2011.

769 Dagsson-Waldhauserova, P., Arnalds, O., and Olafsson, H.: Long-term variability of dust events
770 in Iceland (1949–2011), *Atmos. Chem. Phys.*, 14, 13411–13422, <https://doi.org/10.5194/acp-14-13411-2014>, 2014.

772 DeMott, P. J., Sassen, K., Poellot, M. R., Baumgardner, D., Rogers, D. C., Brooks, S. D., Prenni,
773 A. J., and Kreidenweis, S. M.: African dust aerosols as atmospheric ice nuclei, *Geophys. Res.*
774 *Let.*, 30(14), 1732, <https://doi.org/10.1029/2003GL017410>, 2003.

775 DeMott, P. J., Prenni, A. J., Liu, X., Kreidenweis, S. M., Petters, M. D., Twohy, C. H., Richardson,
776 M. S., Eidhammer, T., and Rogers, D. C.: Predicting global atmospheric ice nuclei distributions
777 and their impacts on climate, *Proc. Natl. Acad. Sci. U.S.A.*, 107(25), 11217–11222,
778 <https://doi.org/10.1073/pnas.0910818107>, 2010.

779 DeMott, P. J., Prenni, A. J., McMeeking, G. R., Sullivan, R. C., Petters, M. D., Tobo, Y., Niemand,
780 M., Möhler, O., Snider, J. R., Wang, Z., and Kreidenweis, S. M.: Integrating laboratory and field
781 data to quantify the immersion freezing ice nucleation activity of mineral dust particles, *Atmos.*
782 *Chem. Phys.*, 15, 393–409, <https://doi.org/10.5194/acp-15-393-2015>, 2015.

783 Dong, X., Xi, B., Crosby, K., Long, C. N., Stone, R. S., and Shupe, M. D.: A 10 year climatology
784 of Arctic cloud fraction and radiative forcing at Barrow, Alaska, *J. Geophys. Res. Atmos.*, 115,
785 D17212, <https://doi.org/10.1029/2009JD013489>, 2010.

786 Dörnbrack, A., Stachlewska, I. S., Ritter, C., and Neuber, R.: Aerosol distribution around Svalbard
787 during intense easterly winds, *Atmos. Chem. Phys.*, 10, 1473–1490, <https://doi.org/10.5194/acp-10-1473-2010>, 2010.

789 Fenn, R. W. and Weickmann, H. K.: Some results of aerosol measurements, *Geofisica Pura e*
790 *Applicata*, 42, 53–61, <https://doi.org/10.1007/BF02113389>, 1959.

791 Gettelman, A. and Morrison, H.: Advanced two-moment bulk microphysics for global models.
792 Part I: off-line tests and comparison with other schemes, *J. Clim.*, 28, 1268–1287,
793 <https://doi.org/10.1175/JCLI-D-14-00102.1>, 2015.

794 Ghan, S. J. and Zaveri, R. A.: Parameterization of optical properties for hydrated internally mixed
795 aerosol, *J. Geophys. Res.*, 112, D10201, <https://doi.org/10.1029/2006JD007927>, 2007.

796 Ginoux, P., Chin, M., Tegen, I., Prospero, J. M., Holben, B., Dubovik, O., and Lin, S.-J.: Sources
797 and distributions of dust aerosols simulated with the GOCART model, *J. Geophys. Res.*, 106,
798 20255–20273, <https://doi.org/10.1029/2000JD000053>, 2001.

Moved down [3]: *Geophys. Res.*

Deleted: Fan, S.-M.: Modeling of observed mineral dust aerosols in the arctic and the impact on winter season low-level clouds, *J.*

Deleted: *Atmos.*, 118, 11161–11174, <https://doi.org/10.1002/jgrd.50842>, 2013.¶

Formatted: Font color: Text 1

Formatted: Font color: Text 1

804 Golaz, J.-C., Larson, V. E., and Cotton, W. R.: A PDF-based model for boundary layer clouds.
805 Part I: Method and model description, *J. Atmos. Sci.*, 59, 3540-3551, <https://doi.org/10.1175/1520->
806 [0469\(2002\)059<3540:APBMFB>2.0.CO;2](https://doi.org/10.1175/1520-0469(2002)059<3540:APBMFB>2.0.CO;2), 2002.

807 Groot Zwaaftink, C. D., Grythe, H., Skov, H., and Stohl, A.: Substantial contribution of northern
808 high-latitude sources to mineral dust in the Arctic, *J. Geophys. Res. Atmos.*, 121, 13678-13697,
809 <https://doi.org/10.1002/2016JD025482>, 2016.

810 Hiranuma, N., Brooks, S. D., Moffet, R. C., Glen, A., Laskin, A., Gilles, M. K.m Liu, P.,
811 Macdonald, A. M., Strapp, J. W., McFarquhar, G. M: Chemical characterization of individual
812 particles and residuals of cloud droplets and ice crystals collected on board research aircraft in the
813 ISDAC 2008 study, *J. Geophys. Res. Atmos.*, 118, 6564-6579, <https://doi.org/10.1002/jgrd.50484>,
814 2013.

815 Hofer, S., Tedstone, A. J., Fettweis, X., and Bamber, J. L.: Cloud microphysics and circulation
816 anomalies control differences in future Greenland melt, *Nat. Clim. Chang.*, 9, 523–528,
817 <https://doi.org/10.1038/s41558-019-0507-8>, 2019.

818 Holben, B. N., Eck, T. F., Slutsker, I., Tanré, D., Buis, J. P., Setzer, A., Vermote, E., Reagan, J.
819 A., Kaufman, Y. J., Nakajima, T., Lavenu, F., Jankowiak, I., and Smirnov, A.: AERONET—A
820 Federated Instrument Network and Data Archive for Aerosol Characterization, *Remote Sens.*
821 *Environ.*, 66, 1–16, [https://doi.org/10.1016/S0034-4257\(98\)00031-5](https://doi.org/10.1016/S0034-4257(98)00031-5), 1998.

822 Hoose, C. and Möhler, O.: Heterogeneous ice nucleation on atmospheric aerosols: a review of
823 results from laboratory experiments, *Atmos. Chem. Phys.*, 12, 9817–9854,
824 <https://doi.org/10.5194/acp-12-9817-2012>, 2012.

825 Huang, Z., Huang, J., Hayasaka, T., Wang, S., Zhou, T., and Jin, H.: Short-cut transport path for
826 Asian dust directly to the Arctic: a case study, *Environ. Res. Lett.*, 10, 114018,
827 <https://doi.org/10.1088/1748-9326/10/11/114018>, 2015.

828 Huneus, N., Schulz, M., Balkanski, Y., Griesfeller, J., Prospero, J., Kinne, S., Bauer, S., Boucher,
829 O., Chin, M., Dentener, F., Diehl, T., Easter, R., Fillmore, D., Ghan, S., Ginoux, P., Grini, A.,
830 Horowitz, L., Koch, D., Krol, M. C., Landing, W., Liu, X., Mahowald, N., Miller, R., Morcrette,
831 J.-J., Myhre, G., Penner, J., Perlwitz, J., Stier, P., Takemura, T., and Zender, C. S.: Global dust
832 model intercomparison in AeroCom phase I, *Atmos. Chem. Phys.*, 11, 7781–7816,
833 <https://doi.org/10.5194/acp-11-7781-2011>, 2011.

834 Irish, V. E., Hanna, S. J., Willis, M. D., China, S., Thomas, J. L., Wentzell, J. J. B., Cirisan, A., Si,
835 M., Leaitch, W. R., Murphy, J. G., Abbatt, J. P. D., Laskin, A., Girard, E., and Bertram, A. K.: Ice
836 nucleating particles in the marine boundary layer in the Canadian Arctic during summer 2014,
837 *Atmos. Chem. Phys.*, 19, 1027–1039, <https://doi.org/10.5194/acp-19-1027-2019>, 2019.

838 Jacob, D. J., Crawford, J. H., Maring, H., Clarke, A. D., Dibb, J. E., Emmons, L. K., Ferrare, R.
839 A., Hostetler, C. A., Russell, P. B., Singh, H. B., Thompson, A. M., Shaw, G. E., McCauley, E.,
840 Pederson, J. R., and Fisher, J. A.: The Arctic Research of the Composition of the Troposphere
841 from Aircraft and Satellites (ARCTAS) mission: design, execution, and first results, *Atmos. Chem.*
842 *Phys.*, 10, 5191–5212, <https://doi.org/10.5194/acp-10-5191-2010>, 2010.

Formatted: Font color: Text 1

843 [Kato, S., Rose, F. G., Rutan, D. A., Thorsen, T. E., Loeb, N. G., Doelling, D. R., Huang, X., Smith,](#)
844 [W. L., Su, W., and Ham, S.-H.: Surface irradiances of Edition 4.0 Clouds and the Earth's Radiant](#)
845 [Energy System \(CERES\) Energy Balanced and Filled \(EBAF\) data product, *J. Climate*, 31, 4501-](#)
846 [4527, <https://doi.org/10.1175/JCLI-D-17-0523.1>, 2018.](#)

847 [Khanal, S., Wang, Z., and French, J. R.: Improving middle and high latitude cloud liquid water](#)
848 [path measurements from MODIS, *Atmos. Res.*, 243, 105033,](#)
849 [https://doi.org/10.1016/j.atmosres.2020.105033, 2020.](#)

850 Kinne, S., Schulz, M., Textor, C., Guibert, S., Balkanski, Y., Bauer, S. E., Bernsten, T., Berglen,
851 T. F., Boucher, O., Chin, M., Collins, W., Dentener, F., Diehl, T., Easter, R., Feichter, J., Fillmore,
852 D., Ghan, S., Ginoux, P., Gong, S., Grini, A., Hendricks, J., Herzog, M., Horowitz, L., Isaksen, I.,
853 Iversen, T., Kirkevåg, A., Kloster, S., Koch, D., Kristjansson, J. E., Krol, M., Lauer, A., Lamarque,
854 J. F., Lesins, G., Liu, X., Lohmann, U., Montanaro, V., Myhre, G., Penner, J., Pitari, G., Reddy,
855 S., Seland, O., Stier, P., Takemura, T., and Tie, X.: An AeroCom initial assessment – optical
856 properties in aerosol component modules of global models, *Atmos. Chem. Phys.*, 6, 1815–1834,
857 <https://doi.org/10.5194/acp-6-1815-2006>, 2006.

858 [Kohfeld, K. E. and Harrison, S. P.: DIRTMAP: the geological record of dust, *Earth-Sci. Rev.*, 54,](#)
859 [81–114, \[https://doi.org/10.1016/S0012-8252\\(01\\)00042-3\]\(https://doi.org/10.1016/S0012-8252\(01\)00042-3\), 2001.](#)

860 Kok, J. F.: A scaling theory for the size distribution of emitted dust aerosols suggests climate
861 models underestimate the size of the global dust cycle, *Proc. Natl. Acad. Sci. U.S.A.*, 108(3),
862 1016–1021, <https://doi.org/10.1073/pnas.1014798108>, 2011.

863 Kok, J. F., Mahowald, N. M., Fratini, G., Gillies, J. A., Ishizuka, M., Leys, J. F., Mikami, M., Park,
864 M.-S., Park, S.-U., Van Pelt, R. S., and Zobeck, T. M.: An improved dust emission model – Part
865 1: Model description and comparison against measurements, *Atmos. Chem. Phys.*, 14, 13023–
866 13041, <https://doi.org/10.5194/acp-14-13023-2014>, 2014a.

867 Kok, J. F., Albani, S., Mahowald, N. M., and Ward, D. S.: An improved dust emission model –
868 Part 2: Evaluation in the Community Earth System Model, with implications for the use of dust
869 source functions, *Atmos. Chem. Phys.*, 14, 13043–13061, [https://doi.org/10.5194/acp-14-13043-](https://doi.org/10.5194/acp-14-13043-2014)
870 [2014](#), 2014b.

871 Kok, J. F., Ridley, D. A., Zhou, Q., Miller, R. L., Zhao, C., Heald, C. L., Ward, D. S., Albani, S.,
872 and Haustein, K.: Smaller desert dust cooling effect estimated from analysis of dust size and
873 abundance, *Nat. Geosci.*, 10, 274–278, <https://doi.org/10.1038/ngeo2912>, 2017.

874 Larson, V. E., Golaz, J.-C., and Cotton, W. R.: Small-Scale and Mesoscale Variability in Cloudy
875 Boundary Layers: Joint Probability Density Functions, *J. Atmos. Sci.*, 59, 3519-3539,
876 [https://doi.org/10.1175/1520-0469\(2002\)059<3519:SSAMVI>2.0.CO;2](https://doi.org/10.1175/1520-0469(2002)059<3519:SSAMVI>2.0.CO;2), 2002.

877 Liu, X., Xie, S., Boyle, J., Klein, S. A., Shi, X., Wang, Z., Lin, W., Ghan, S. J., Earle, M., Liu, P.,
878 S. K., and Zelenyuk, A.: Testing cloud microphysics parameterizations in NCAR CAM5 with
879 ISDAC and M-PACE observations, *J. Geophys. Res.*, 116, D00T11,
880 <https://doi.org/10.1029/2011JD015889>, 2011.

Formatted: Font color: Text 1

881 Liu, X., Ma, P.-L., Wang, H., Tilmes, S., Singh, B., Easter, R. C., Ghan, S. J., and Rasch, P. J.:
882 Description and evaluation of a new four-mode version of the Modal Aerosol Module (MAM4)
883 within version 5.3 of the Community Atmosphere Model, *Geosci. Model Dev.*, 9, 505–522,
884 <https://doi.org/10.5194/gmd-9-505-2016>, 2016.

885 [Loeb, N. G., Doelling, D. R., Wang, H., Su, W., Nguyen, C., Corbett, J. G., Liang, L., Mitrescu,](#)
886 [C., Rose, F. G., and Kato, S.: Clouds and the Earth’s Radiant Energy System \(CERES\) Energy](#)
887 [Balanced and Filled \(EBAF\) Top-of-Atmosphere \(TOA\) Edition-4.0 Data Product. *J. Climate*, 31,](#)
888 [895-918, <https://doi.org/10.1175/JCLI-D-17-0208.1>, 2018.](#)

889 Luo, C., Mahowald, N. M., and Corral, J. del: Sensitivity study of meteorological parameters on
890 mineral aerosol mobilization, transport, and distribution, *J. Geophys. Res.*, 108, 4447,
891 <https://doi.org/10.1029/2003JD003483>, 2003.

892 Luo, T., Wang, Z., Ferrare, R. A., Hostetler, C. A., Yuan, R., and Zhang, D.: Vertically resolved
893 separation of dust and other aerosol types by a new lidar depolarization method, *Opt. Express*, 23,
894 14095-14107, <https://doi.org/10.1364/OE.23.014095>, 2015a.

895 Luo, T., Wang, Z., Zhang, D., Liu, X., Wang, Y., and Yuan, R.: Global dust distribution from
896 improved thin dust layer detection using A-train satellite lidar observations, *Geophys. Res. Lett.*,
897 42, 620–628, <https://doi.org/10.1002/2014GL062111>, 2015b.

898 Maenhaut, W., Fernandez-Jimenez, M.-T., Rajta, I., Dubtsov, S., Meixner, F. X., Andreae, M. O.,
899 Torr, S., Hargrove, J. W., Chimanga, P., and Mlambo, J.: Long-term aerosol composition
900 measurements and source apportionment at Rukomechi, Zimbabwe, *J. Aerosol Sci.*, 31(Suppl. 1),
901 S469–S470, 2000a.

902 Maenhaut, W., Fernandez-Jimenez, M.-T., Vanderzalm, J. L., Hooper, B. M., Hooper, M. A., and
903 Tapper, N. J.: Aerosol composition at Jabiru, Australia and impact of biomass burning, *J. Aerosol*
904 *Sci.*, 31(Suppl. 1), S745–S746, 2000b.

905 Mahowald, N. M., Engelstaedter, S., Luo, C., Sealy, A., Artaxo, P., Benitez-Nelson, C., Bonnet,
906 S., Chen, Y., Chuang, P. Y., Cohen, D. D., Dulac, F., Herut, B., Johansen, A. M., Kubilay, N.,
907 Losno, R., Maenhaut, W., Paytan, A., Prospero, J. M., Shank, L. M., and Siefert, R. L.:
908 Atmospheric iron deposition: global distribution, variability, and human perturbations, *Ann. Rev.*
909 *Mar. Sci.*, 1, 245–278, <https://doi.org/10.1146/annurev.marine.010908.163727>, 2009.

910 Mason, R. H., Si, M., Chou, C., Irish, V. E., Dickie, R., Elizondo, P., Wong, R., Brintnell, M.,
911 Elsasser, M., Lassar, W. M., Pierce, K. M., Leitch, W. R., MacDonald, A. M., Platt, A., Toom-
912 Saunry, D., Sarda-Estève, R., Schiller, C. L., Suski, K. J., Hill, T. C. J., Abbatt, J. P. D., Huffman,
913 J. A., DeMott, P. J., and Bertram, A. K.: Size-resolved measurements of ice-nucleating particles
914 at six locations in North America and one in Europe, *Atmos. Chem. Phys.*, 16, 1637–1651,
915 <https://doi.org/10.5194/acp-16-1637-2016>, 2016.

916 McCluskey, C. S., Ovadnevaite, J., Rinaldi, M., Atkinson, J., Belosi, F., Ceburnis, D., Marullo, S.,
917 Hill, T. C. J., Lohmann, U., Kanji, Z. A., O’Dowd, C., Kreidenweis, S. M., and DeMott, P. J.:
918 Marine and terrestrial organic ice-nucleating particles in pristine marine to continentally

Formatted: Font color: Text 1

919 influenced Northeast Atlantic air masses, *J. Geophys. Res. Atmos.*, 123, 6196–6212,
920 <https://doi.org/10.1029/2017JD028033>, 2018.

921 McFarquhar, G. M., Ghan, S., Verlinde, J., Korolev, A., Strapp, J. W., Schmid, B., Tomlinson, J.
922 M., Wolde, M., Brooks, S. D., Cziczo, D., Dubey, M. K., Fan, J., Flynn, C., Gultepe, I., Hubbe, J.,
923 Gilles, M. K., Laskin, A., Lawson, P., Leaitch, W. R., Liu, P., Liu, X., Lubin, D., Mazzoleni, C.,
924 Macdonald, A.-M., Moffet, R. C., Morrison, H., Ovchinnikov, M., Shupe, M. D., Turner, D. D.,
925 Xie, S., Zelenyuk, A., Bae, K., Freer, M., and Glen, A.: Indirect and Semi-direct Aerosol
926 Campaign: The Impact of Arctic Aerosols on Clouds, *Bull. Amer. Meteor. Soc.*, 92, 183–201,
927 <https://doi.org/10.1175/2010BAMS2935.1>, 2011.

928 Morrison, H., de Boer, G., Feingold, G., Harrington, J., Shupe, M. D., and Sulia, K.: Resilience of
929 persistent Arctic mixed-phase clouds, *Nat. Geosci.*, 5, 11–17, <https://doi.org/10.1038/ngeo1332>,
930 2012.

931 Murray, B. J., O’Sullivan, D., Atkinson, J. D., and Webb, M. E.: Ice nucleation by particles
932 immersed in supercooled cloud droplets, *Chem. Soc. Rev.*, 41, 6519–6554,
933 <https://doi.org/10.1039/c2cs35200a>, 2012.

934 Paramonov, M., David, R. O., Kretzschmar, R., and Kanji, Z. A.: A laboratory investigation of the
935 ice nucleation efficiency of three types of mineral and soil dust, *Atmos. Chem. Phys.*, 18, 16515–
936 16536, <https://doi.org/10.5194/acp-18-16515-2018>, 2018.

937 [Platnick, S., King, M. D., Ackerman, S. A., Menzel, W. P., Baum, B. A., Riédi, J. C., & Frey, R.](#)
938 [A.: The MODIS cloud products: Algorithms and examples from terra, *IEEE Trans. Geosci.*](#)
939 [*Remote Sens.*, 41\(2\), 459–472. <https://doi.org/10.1109/TGRS.2002.808301>](#)

940 Prenni, A. J., Harrington, J. Y., Tjernström, M., DeMott, P. J., Avramov, A., Long, C. N.,
941 Kreidenweis, S. M., Olsson, P. Q., and Verlinde, J.: Can ice-nucleating aerosols affect Arctic
942 seasonal climate?, *Bull. Amer. Meteor. Soc.*, 88, 541–550, [https://doi.org/10.1175/BAMS-88-4-](https://doi.org/10.1175/BAMS-88-4-541)
943 541, 2007.

944 Prenni, A. J., Demott, P. J., Rogers, D. C., Kreidenweis, S. M., Mcfarquhar, G. M., Zhang, G., and
945 Poellot, M. R.: Ice nuclei characteristics from M-PACE and their relation to ice formation in
946 clouds, *Tellus B*, 61, 436–448, <https://doi.org/10.1111/j.1600-0889.2009.00415.x>, 2009.

947 Prospero, J. M.: The Atmospheric Transport of Particles to the Ocean, in: *Particle Flux in the*
948 *Ocean*, edited by: Ittekkot, V., Sch’afner, P., Honjo, S., and Depetris, P. J., John Wiley & Sons Ltd.,
949 New York, 1996.

950 Prospero, J. M., Bullard, J. E., and Hodgkins, R.: High-Latitude Dust Over the North Atlantic:
951 Inputs from Icelandic Proglacial Dust Storms, *Science*, 335, 1078–1082,
952 <https://doi.org/10.1126/science.1217447>, 2012.

953 Prospero, J. M., Uematsu, M., and Savoie, D. L.: Mineral aerosol transport to the Pacific Ocean,
954 edited by: Riley, J. P., 187–218, Academic Press, New York, 1989.

Formatted: Font color: Text 1

955 Rasch, P. J., Xie, S., Ma, P. -L., Lin, W., Wang, H., Tang, Q., Burrows, S. M., Caldwell, P., Zhang,
956 K., Easter, R. C., Cameron-Smith, P., Singh, B., Wan, H., Golaz, J. -C., Harrop, B. E., Roesler, E.,
957 Bacmeister, J., Larson, V. E., Evans, K. J., Qian, Y., Taylor, M., Leung, L. R., Zhang, Y., Brent,
958 L., Branstetter, M., Hannay, C., Mahajan, S., Mامتjanov, A., Neale, R., Richter, J. H., Yoon, J.
959 -H., Zender, C. S., Bader, D., Flanner, M., Foucar, J. G., Jacob, R., Keen, N., Klein, S. A., Liu, X.,
960 Salinger, A. G., Shrivastava, M., and Yang, Y.: An overview of the atmospheric component of the
961 Energy Exascale Earth System Model, *J. Adv. Model. Earth Syst.*, 11, 2377–2411,
962 <https://doi.org/10.1029/2019MS001629>, 2019.

963 Ridley, D. A., Heald, C. L., Kok, J. F., and Zhao, C.: An observationally constrained estimate of
964 global dust aerosol optical depth, *Atmos. Chem. Phys.*, 16, 15097–15117,
965 <https://doi.org/10.5194/acp-16-15097-2016>, 2016.

966 Sanchez-Marroquin, A., Arnalds, O., Baustian-Dorsi, K. J., Browse, J., Dagsson-Waldhauserova,
967 P., Harrison, A. D., Maters, E. C., Pringle, K. J., Vergara-Temprado, J., Burke, I. T., McQuaid, J.
968 B., Carslaw, K. S., and Murray, B. J.: Iceland is an episodic source of atmospheric ice-nucleating
969 particles relevant for mixed-phase clouds, *Sci. Adv.*, 6, eaba8137,
970 <https://doi.org/10.1126/sciadv.aba8137>, 2020.

971 Schill, G. P., DeMott, P. J., Emerson, E. W., Rauker, A. M. C., Kodros, J. K., Suski, K. J., Hill, T.
972 C. J., Levin, E. J. T., Pierce, J. R., Farmer, D. K., and Kreidenweis, S. M.: The contribution of
973 black carbon to global ice nucleating particle concentrations relevant to mixed-phase clouds, *Proc.*
974 *Natl. Acad. Sci. U.S.A.*, 117, 22705–22711, <https://doi.org/10.1073/pnas.2001674117>, 2020.

975 [Schweiger, A. J., Lindsay, R. W., Vavrus, S., and Francis, J. A.: Relationships between Arctic sea](#)
976 [ice and clouds dusting autumn, *J. Clim.*, 21, 4799-4810, <https://doi.org/10.1175/2008JCLI2156.1>](#)

977 [Shao, Y., Wyrwoll, K.-H., Chappell, A., Huang, J., Lin, Z., McTainsh, G. H., Mikami, M., Tanaka,](#)
978 [T. Y., Wang, X., and Yoon, S.: Dust cycle: An emerging core theme in Earth system science,](#)
979 [*Aeolian Res.*, 2, 181–204, <https://doi.org/10.1016/j.aeolia.2011.02.001>, 2011.](#)

980 Shi, Y. and Liu, X.: Dust Radiative Effects on Climate by Glaciating Mixed-Phase Clouds,
981 *Geophys. Res. Lett.*, 46, 6128–6137, <https://doi.org/10.1029/2019GL082504>, 2019.

982 Shupe, M. D. and Intrieri, J. M.: Cloud Radiative Forcing of the Arctic Surface: The Influence of
983 Cloud Properties, Surface Albedo, and Solar Zenith Angle, *J. Clim.*, 17, 616–628,
984 [https://doi.org/10.1175/1520-0442\(2004\)017<0616:CRFOTA>2.0.CO;2](https://doi.org/10.1175/1520-0442(2004)017<0616:CRFOTA>2.0.CO;2), 2004.

985 Si, M., Evoy, E., Yun, J., Xi, Y., Hanna, S. J., Chivulescu, A., Rawlings, K., Veber, D., Platt, A.,
986 Kunkel, D., Hoor, P., Sharma, S., Leaitch, W. R., and Bertram, A. K.: Concentrations,
987 composition, and sources of ice-nucleating particles in the Canadian High Arctic during spring
988 2016, *Atmos. Chem. Phys.*, 19, 3007–3024, <https://doi.org/10.5194/acp-19-3007-2019>, 2019.

989 [Sirois, A., and Barrie, L. A.: Arctic lower tropospheric aerosol trends and composition at Alert,](#)
990 [Canada: 1980-1995, *J. Geophys. Res. Atmos.*, 104, 11599-11618,](#)
991 [<https://doi.org/10.1029/1999JD900077>, 1999.](#)

Formatted: Font color: Text 1

Moved (insertion) [3]

Formatted: Font color: Text 1

992 [Smirnov, A., Holben, B. N., Eck, T. F., Dubovik, O., and Slutsker, I.: Cloud screening and quality](#)
993 [control algorithms for the AERONET database, Remote Sens. Environ., 73, 337–349,](#)
994 [https://doi.org/10.1016/S0034-4257\(00\)00109-7](https://doi.org/10.1016/S0034-4257(00)00109-7), 2000.

995 [Stohl, A.: Characteristics of atmospheric transport into the Arctic troposphere, J. Geophys. Res.,](#)
996 [111, D11306, https://doi.org/10.1029/2005JD006888](https://doi.org/10.1029/2005JD006888), 2006.

997 Stone, R., Anderson, G., Andrews, E., Dutton, E., Harris, J., Shettle, E., Berk, A.: Asian dust
998 signatures at Barrow: observed and simulated. Incursions and impact of Asian dust over Northern
999 Alaska, Workshop on Remote Sensing of Atmospheric Aerosols, IEEE Workshop on Remote
1000 Sensing of Atmospheric Aerosols, 74-79, <https://doi.org/10.1109/AERSOL.2005.1494152>, 2005.

1001 [Tan, I. and Storelvmo, T.: Sensitivity study on the influence of cloud microphysical parameters on](#)
1002 [mixed-phase cloud thermodynamic phase partitioning in CAM5. J. Atmos. Sci., 73, 709-728,](#)
1003 <https://doi.org/10.1175/JAS-D-15-0152.1>, 2016.

1004 [Tan, I. and Storelvmo, T.: Evidence of Strong Contributions from Mixed-Phase Clouds to Arctic](#)
1005 [Climate Change, Geophys. Res. Lett., 46, 2894–2902, https://doi.org/10.1029/2018GL081871,](#)
1006 2019.

1007 Tanaka, T. Y. and Chiba, M.: A numerical study of the contributions of dust source regions to the
1008 global dust budget, *Glob. Planet. Change*, 52, 88–104,
1009 <https://doi.org/10.1016/j.gloplacha.2006.02.002>, 2006.

1010 Tegen, I., Harrison, S. P., Kohfeld, K., Prentice, I. C., Coe, M., and Heimann, M.: Impact of
1011 vegetation and preferential source areas on global dust aerosol: Results from a model study, *J.*
1012 *Geophys. Res. Atmos.*, 107, AAC 14-1-AAC 14-27, <https://doi.org/10.1029/2001JD000963>, 2002.

1013 Tobo, Y., Adachi, K., DeMott, P. J., Hill, T. C. J., Hamilton, D. S., Mahowald, N. M., Nagatsuka,
1014 N., Ohata, S., Uetake, J., Kondo, Y., and Koike, M.: Glacially sourced dust as a potentially
1015 significant source of ice nucleating particles, *Nat. Geosci.*, 12, 253–258,
1016 <https://doi.org/10.1038/s41561-019-0314-x>, 2019.

1017 Vali, G.: Nucleation terminology, *Bull. Am. Meteorol. Soc.*, 66, 1426–1427, 1985.

1018 Vali, G., DeMott, P. J., Möhler, O., and Whale, T. F.: Technical Note: A proposal for ice nucleation
1019 terminology, *Atmos. Chem. Phys.*, 15, 10263–10270, <https://doi.org/10.5194/acp-15-10263-2015>,
1020 2015.

1021 VanCuren, R. A., Cahill, T., Burkhart, J., Barnes, D., Zhao, Y., Perry, K., Cliff, S., and McConnell,
1022 J.: Aerosols and their sources at Summit Greenland – First results of continuous size- and time-
1023 resolved sampling, *Atmos. Environ.*, 52, 82–97, <https://doi.org/10.1016/j.atmosenv.2011.10.047>,
1024 2012.

1025 Wang, H., Rasch, P. J., Easter, R. C., Singh, B., Zhang, R., Ma, P.-L., Qian, Y., Ghan, S. J., and
1026 Beagley, N.: Using an explicit emission tagging method in global modeling of source-receptor
1027 relationships for black carbon in the Arctic: Variations, sources, and transport pathways, *J.*
1028 *Geophys. Res. Atmos.*, 119, 12888-12909, <https://doi.org/10.1002/2014JD022297>, 2014.

Formatted: Font color: Text 1

Formatted: Font color: Text 1

- 1029 Wang, H., Easter, R. C., Zhang, R., Ma, P.-L., Singh, B., Zhang, K., Ganguly, D., Rasch, P. J.,
1030 Burrows, S. M., Ghan, S. J., Lou, S., Qian, Y., Yang, Y., Feng, Y., Flanner, M., Leung, L. R., Liu,
1031 X., Shrivastava, M., Sun, J., Tang, Q., Xie, S., and Yoon, J.: Aerosols in the E3SM Version 1:
1032 New Developments and Their Impacts on Radiative Forcing, *J. Adv. Model. Earth Syst.*, 12,
1033 e2019MS001851, <https://doi.org/10.1029/2019MS001851>, 2020.
- 1034 Wang, Y., Liu, X., Hoose, C., and Wang, B.: Different contact angle distributions for
1035 heterogeneous ice nucleation in the Community Atmospheric Model version 5, *Atmos. Chem.*
1036 *Phys.*, 14, 10411–10430, <https://doi.org/10.5194/acp-14-10411-2014>, 2014.
- 1037 Westbrook, C. D. and Illingworth, A. J.: The formation of ice in a long-lived supercooled layer
1038 cloud: Ice Formation in Altocumulus, *Q. J. R. Meteorol. Soc.*, 139, 2209–2221,
1039 <https://doi.org/10.1002/qj.2096>, 2013.
- 1040 Wilson, T. W., Ladino, L. A., Alpert, P. A., Breckels, M. N., Brooks, I. M., Browse, J., Burrows,
1041 S. M., Carslaw, K. S., Huffman, J. A., Judd, C., Kilhau, W. P., Mason, R. H., McFiggans, G.,
1042 Miller, L. A., Nájera, J. J., Polishchuk, E., Rae, S., Schiller, C. L., Si, M., Vergara-Temprado, J.,
1043 Whale, T. F., Wong, J. P. S., Wurl, O., Yakobi-Hancock, J. D., Abbatt, J. P. D., Aller, J. Y.,
1044 Bertram, A. K., Knopf, D. A., and Murray, B. J.: A marine biogenic source of atmospheric ice-
1045 nucleating particles, *Nature*, 525, 234–238, <https://doi.org/10.1038/nature14986>, 2015.
- 1046 [Winker, D. M., Tackett, J. L., Getzewich, B. J., Liu, Z., Vaughan, M. A., and Rogers, R. R.: The](#)
1047 [global 3-D distribution of tropospheric aerosols as characterized by CALIOP, *Atmos. Chem. Phys.*](#)
1048 [13, 3345–3361, <https://doi.org/10.5194/acp-13-3345-2013>, 2013.](#)
- 1049 Wu, M., Liu, X., Yu, H., Wang, H., Shi, Y., Yang, K., Darmenov, A., Wu, C., Wang, Z., Luo, T.,
1050 Feng, Y., and Ke, Z.: Understanding processes that control dust spatial distributions with global
1051 climate models and satellite observations, *Atmos. Chem. Phys.*, 20, 13835–13855,
1052 <https://doi.org/10.5194/acp-20-13835-2020>, 2020.
- 1053 Yang, Y., Wang, H., Smith, S. J., Easter, R., Ma, P.-L., Qian, Y., Yu, H., Li, C., and Rasch, P. J.:
1054 Global source attribution of sulfate concentration and direct and indirect radiative forcing, *Atmos.*
1055 *Chem. Phys.*, 17, 8903–8922, <https://doi.org/10.5194/acp-17-8903-2017>, 2017a.
- 1056 Yang, Y., Wang, H., Smith, S. J., Ma, P.-L., and Rasch, P. J.: Source attribution of black carbon
1057 and its direct radiative forcing in China, *Atmos. Chem. Phys.*, 17, 4319–4336,
1058 <https://doi.org/10.5194/acp-17-4319-2017>, 2017b.
- 1059 Yang, Y., Wang, H., Smith, S. J., Zhang, R., Lou, S., Yu, H., Li, C., and Rasch, P. J.: Source
1060 Apportionments of Aerosols and Their Direct Radiative Forcing and Long-Term Trends Over
1061 Continental United States, *Earth's Future*, 6, 793–808, <https://doi.org/10.1029/2018EF000859>,
1062 2018.
- 1063 Zender, C. S., Bian, H., and Newman, D.: Mineral Dust Entrainment and Deposition (DEAD)
1064 model: Description and 1990s dust climatology, *J. Geophys. Res.*, 108, 4416,
1065 <https://doi.org/10.1029/2002JD002775>, 2003.

Formatted: Font color: Text 1

1066 Zhang, G. J. and McFarlane, N. A.: Sensitivity of climate simulations to the parameterization of
1067 cumulus convection in the Canadian climate centre general circulation model, *Atmos.-Ocean*, 33,
1068 407–446, <https://doi.org/10.1080/07055900.1995.9649539>, 1995.

1069 Zhang, K., Wan, H., Liu, X., Ghan, S. J., Kooperman, G. J., Ma, P.-L., Rasch, P. J., Neubauer, D.,
1070 and Lohmann, U.: Technical Note: On the use of nudging for aerosol–climate model
1071 intercomparison studies, *Atmos. Chem. Phys.*, 14, 8631–8645, [https://doi.org/10.5194/acp-14-](https://doi.org/10.5194/acp-14-8631-2014)
1072 8631-2014, 2014.

1073 Zhang, M., Liu, X., Diao, M., D’Alessandro, J. J., Wang, Y., Wu, C., Zhang, D., Wang, Z., and
1074 Xie, S.: Impacts of representing heterogeneous distribution of cloud liquid and ice on phase
1075 partitioning of Arctic mixed-phase clouds with NCAR CAM5, *J. Geophys. Res. Atmos.*, 124,
1076 13071–13090, <https://doi.org/10.1029/2019JD030502>, 2019.

1077 Zhang, M., Xie, S., Liu, X., Lin, W., Zhang, K., Ma, H.-Y., Zheng, X., and Zhang, Y.: Toward
1078 understanding the simulated phase partitioning of Arctic single-layer mixed-phase clouds in
1079 E3SM, *Earth Space Sci.*, 7, e2020EA001125, <https://doi.org/10.1029/2020EA001125>, 2020.

1080 Zhang, Y., Xie, S., Lin, W., Klein, S. A., Zelinka, M., Ma, P., Rasch, P. J., Qian, Y., Tang, Q., and
1081 Ma, H.: Evaluation of clouds in version 1 of the E3SM atmosphere model with satellite simulators,
1082 *J. Adv. Model. Earth Syst.*, 11, 1253–1268, <https://doi.org/10.1029/2018MS001562>, 2019.

1083 Zhao, X. and Liu, X.: Global Importance of Secondary Ice Production, *Geophys. Res. Lett.*, 48,
1084 e2021GL092581, <https://doi.org/10.1029/2021GL092581>, 2021.

1085 Zhao, X., Liu, X., Burrows, S. M., and Shi, Y.: Effects of marine organic aerosols as sources of
1086 immersion-mode ice-nucleating particles on high-latitude mixed-phase clouds, *Atmos. Chem.*
1087 *Phys.*, 21, 2305–2327, <https://doi.org/10.5194/acp-21-2305-2021>, 2021a.

1088 Zhao, X., Liu, X., Phillips, V. T. J., and Patade, S.: Impacts of secondary ice production on Arctic
1089 mixed-phase clouds based on ARM observations and CAM6 single-column model simulations,
1090 *Atmos. Chem. Phys.*, 21, 5685–5703, <https://doi.org/10.5194/acp-21-5685-2021>, 2021b.

1091

1092

Table 1. Experiments conducted in this study.

Experiment	Description
CTRL	Control simulation using the CNT parameterization for heterogeneous ice nucleation and Kok et al. (2014a, b) for dust emission parameterization.
noArc	Same as CTRL, but turn off heterogeneous ice nucleation in mixed-phase clouds by HLD.
noNAf	Same as CTRL, but turn off heterogeneous ice nucleation in mixed-phase clouds by North African dust.
noEAs	Same as CTRL, but turn off heterogeneous ice nucleation in mixed-phase clouds by East Asian dust.

1093

Formatted: Heading 1, Line spacing: single

Formatted: Font: Not Bold

1094
1095
1096

Table 2. Annual and seasonal mean Arctic dust burden (mg m^{-2}) from different sources. The numbers in parentheses are the relative contributions (%) of each source to the total Arctic dust burden. The total Arctic dust burden is shown in the last row.

	ANN	MAM	JJA	SON	DJF
Arc	2.1 (30.7)	0.3 (3.9)	5.1 (50.4)	2.5 (47.5)	0.5 (14.6)
NAm	0.1 (0.9)	0.1 (1.3)	0.1 (0.6)	0.0 (0.7)	0.0 (1.2)
NAf	1.7 (24.2)	3.7 (41.4)	1.5 (14.4)	0.7 (12.9)	0.9 (26.4)
CAs	0.9 (12.8)	1.1 (12.5)	1.3 (13.0)	0.8 (14.7)	0.3 (10.1)
MSA	0.8 (11.5)	1.6 (17.9)	0.7 (7.0)	0.3 (6.1)	0.6 (17.4)
EAs	1.4 (19.9)	2.0 (23.0)	1.5 (14.7)	0.9 (18.1)	1.0 (30.2)
RoW	0.0 (0.0)	0.0 (0.0)	0.0 (0.0)	0.0 (0.0)	0.0 (0.1)
Total Burden (mg m^{-2})	6.9	8.9	10.2	5.2	3.3

1097

Formatted: Heading 1, Line spacing: single

Formatted: Font: Not Bold

1098 **Table 3.** Summary of the nine Arctic INP measurements used for INP comparisons in Figure 8.

Formatted: Font: Not Bold

Formatted: Heading 1, Line spacing: single

Location	Time period	Measured platform	Reference	Possible INP source mentioned in literature	INP source attribution from modeling ⁺
A Utqiagvik	Apr. 2008 (spring)	Aircraft	McFarquhar et al. (2011)	Metallic or composed of dust*	LLD (EAs)
B Alert	Mar. - May 2014 (spring)	Ground-based	Mason et al. (2016)	Not mentioned	LLD (EAs)
C Alert	Mar. 2016 (spring)	Ground-based	Si et al. (2019)	LLD from Gobi Desert	LLD (EAs)
D Zeppelin	Mar. 2017 (spring)	Ground-based	Tobo et al. (2019)	Marine organic aerosols	HLD (NEu)
E Oliktok Point	Mar. - May 2017 (spring)	Ground-based	Creamean et al. (2018)	Dust and primary marine aerosols	LLD (mainly from EAs and some from NAF)
F Alert	Jun. - Jul. 2014 (summer)	Ground-based	Mason et al. (2016)	Not mentioned	HLD (NCa)
G Zeppelin	Jul. 2016 (summer)	Ground-based	Tobo et al. (2019)	HLD from Svalbard or other high latitude sources**	HLD (NEu)
H Utqiagvik	Oct. 2004 (autumn)	Aircraft	Prenni et al. (2007)	Dust and carbonaceous particles	HLD (NCa) and LLD (EAs)
South of Iceland	Oct. 2014 (autumn)	Aircraft	Sanchez-Marroquin et al. (2020)	Icelandic dust	Dominated by HLD (GrI), little from LLD (NAf)

Deleted: Spring,

Deleted: HLD (NCa) and

Deleted: Spring,

Deleted: Spring,

Deleted: Spring,

Deleted: Spring,

Deleted: Summer,

Deleted: Summer,

Deleted: Autumn,

Deleted: Autumn,

1099 ⁺ The modeling analyses include INP contribution from HLD (using SM20), LLD (using D15),
 1100 BC, and SSA. The

1101 * Carbonate, black carbon, and organic may also contribute, according to Hiranuma et al. (2013).

1102 ** The HLD in this campaign is reported to have remarkably high ice nucleating ability, which may
 1103 be related to the presence of organic matter.

1104

Deleted: ⁺ The modeling analyses include INP contribution from HLD, LLD, BC, and SSA.

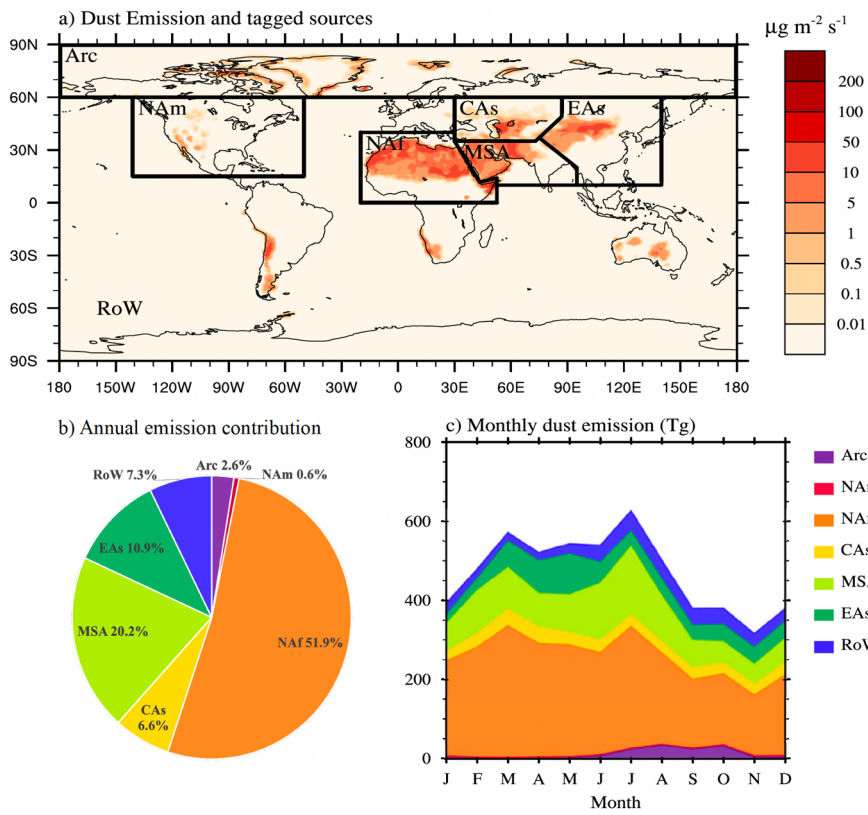
1117 **Table 4.** Arctic averaged surface downwelling radiative fluxes and TOA cloud radiative forcing
 1118 changes caused by dust INPs originated from local Arctic sources (Arc), North Africa (NAf), and
 1119 East Asia (EAs). Units are $W m^{-2}$.

Formatted: Heading 1, Left, Line spacing: single

Formatted: Font: Not Bold

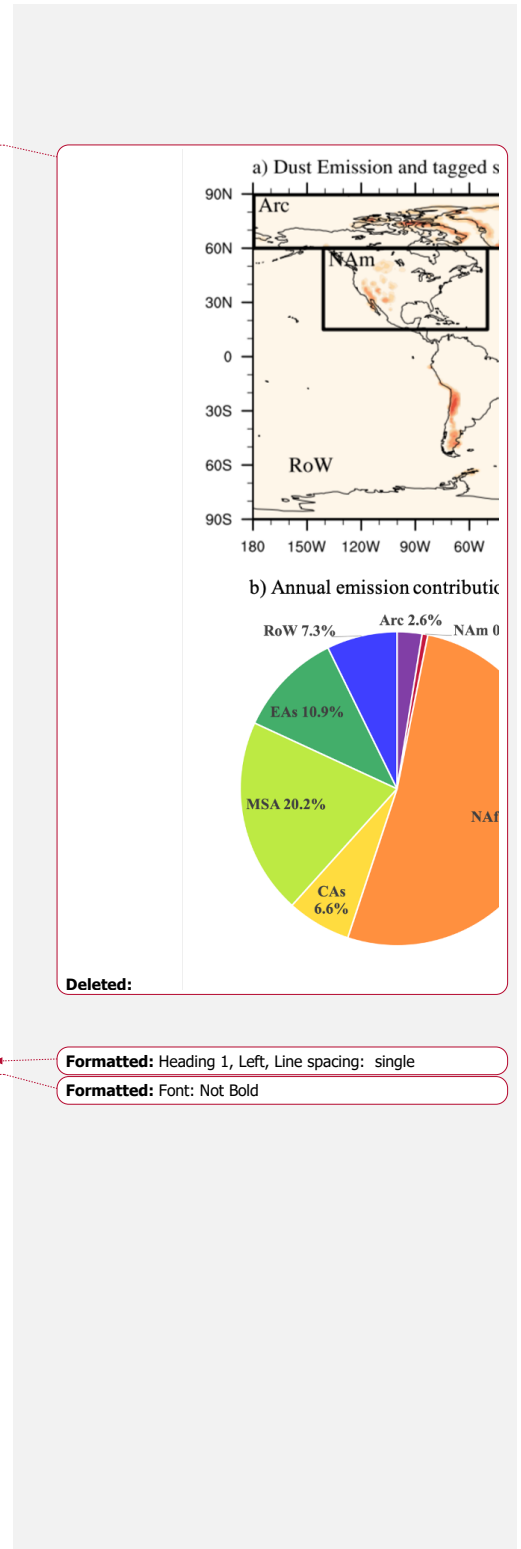
	ANN			MAM			JJA			SON			DJF		
	SW	LW	Net	SW	LW	Net	SW	LW	Net	SW	LW	Net	SW	LW	Net
Part 1. INP effect on surface downwelling radiative fluxes															
Arc	0.11	-0.36	-0.24	0.27	-0.31	-0.03	0.12	0	0.12	0.04	-0.55	-0.51	0.02	-0.56	-0.54
NAf	0.33	-0.25	0.08	0.78	-0.60	0.19	0.50	0.01	0.51	0.02	-0.03	-0.02	0.03	-0.39	-0.36
EAs	0.35	-0.41	-0.06	0.68	-0.60	0.09	0.59	0.02	0.61	0.08	-0.27	-0.19	0.04	-0.80	-0.76
Part 2. INP effect on TOA cloud radiative forcing															
Arc	0.06	-0.11	-0.05	0.06	-0.07	-0.01	0.14	-0.02	0.12	0.03	-0.23	-0.20	0.01	-0.12	-0.11
NAf	0.20	-0.23	-0.03	0.34	-0.34	0	0.41	-0.18	0.24	0.03	-0.20	-0.16	0.02	-0.23	-0.21
EAs	0.20	-0.24	-0.04	0.22	-0.23	-0.02	0.46	-0.17	0.29	0.09	-0.29	-0.20	0.02	-0.26	-0.24

1120



1121

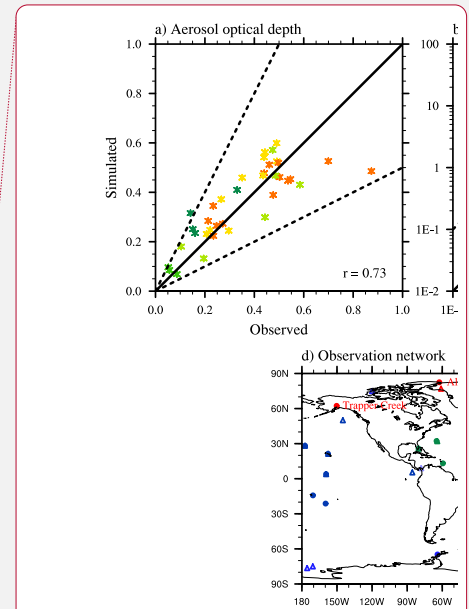
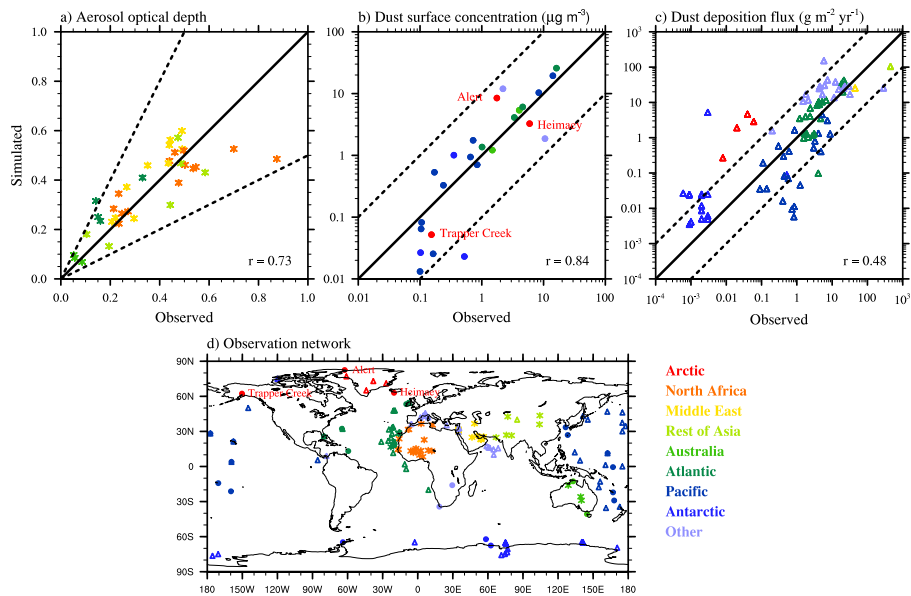
1122 **Figure 1.** a) Simulated global annual mean dust emission with 7 tagged source regions (Arc: Arctic; NAM: North America; NAF: North Africa; CAs: Central Asia; MSA: Middle East and
 1123 South Asia; EAs: East Asia; RoW: Rest of the World). b) The respective percentage contributions
 1124 to the global annual mean dust emission from the individual source regions. c) Seasonal cycle of
 1125 global dust emission.
 1126



Deleted:

Formatted: Heading 1, Left, Line spacing: single

Formatted: Font: Not Bold



1128

1129 **Figure 2.** Comparison of observed and simulated a) averaged AOD at 40 dust-dominated stations
 1130 (stars), b) dust surface concentration at 25 sites (circles), and c) dust deposition flux at 84 sites
 1131 (triangles). Solid lines represent 1:1 comparison. Dashed lines mark 2 factor of magnitude bias in
 1132 panel a) and 1 order of magnitude differences in panel b) and c). For each comparison, the
 1133 correlation coefficient (r) is noted. The AOD data is conducted by AERONET. The dust surface
 1134 concentration measurements include 20 stations managed by Rosenstiel School of Marine and
 1135 Atmospheric Science at the University of Miami (Prospero et al., 1989; Prospero, 1996; Arimoto
 1136 et al., 1995), two Australia stations (Maenhaut et al., 2000a, b), and three Arctic stations (Heimay
 1137 (Prospero et al., 2012), Alert (Sirois and Barrie, 1999), and Trapper Creek (IMPROVE)). The
 1138 deposition fluxes data is a compilation of measurements from Ginoux et al. (2001), Mahowald et
 1139 al. (2009), and the Dust Indicators and Records in Terrestrial and Marine Paleoenvironments
 1140 (DIRTMAP) database (Tegen et al., 2002; Kohfeld and Harrison, 2001). Stations are grouped
 1141 regionally and classified by different colors. The locations of the measurements are shown in panel
 1142 d).

1143

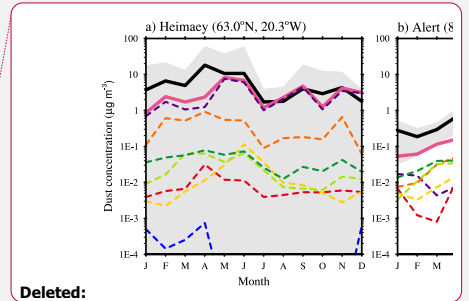
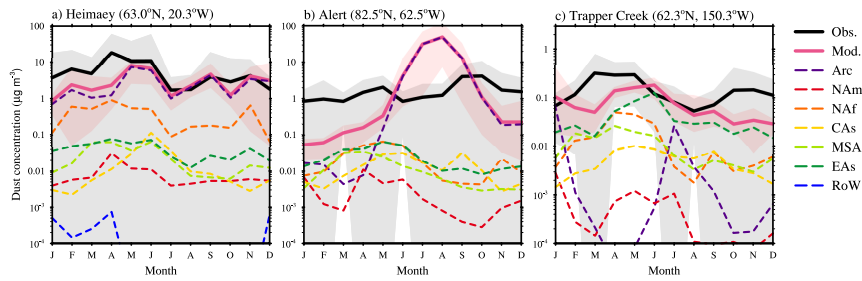
Deleted:

Formatted: Heading 1, Left, Line spacing: single

Formatted: Font: Not Bold

Deleted: Fan, 2013

Formatted: Font: Not Bold



Deleted:

1146

1147 **Figure 3.** Comparison of measured (black solid line, with gray shade representing standard
 1148 deviation) and simulated (pink solid line, with pink shade representing year-to-year variability)
 1149 monthly mean dust surface concentration at three high latitude stations – a) Heimaey, b) Alert, and
 1150 c) Trapper Creek. The model results are averaged from year 2007 to 2011. Contributions from
 1151 seven tagged sources are shown by colored dashed lines. The locations of the three stations are
 1152 shown in Figure 2d. The measurements at Heimaey (Prospero et al., 2012), Alert (Sirois and Barrie,
 1153 1999), and Trapper Creek (IMPROVE) are averaged for the years 1997 to 2002, 1980 to 1995, and
 1154 2007 to 2011, respectively. The dust concentrations at Trapper Creek only include particles with
 1155 diameter less than 2.5 µm. The other two stations include dust over the whole size range.

Formatted: Heading 1, Left, Line spacing: single

Formatted: Font: Not Bold

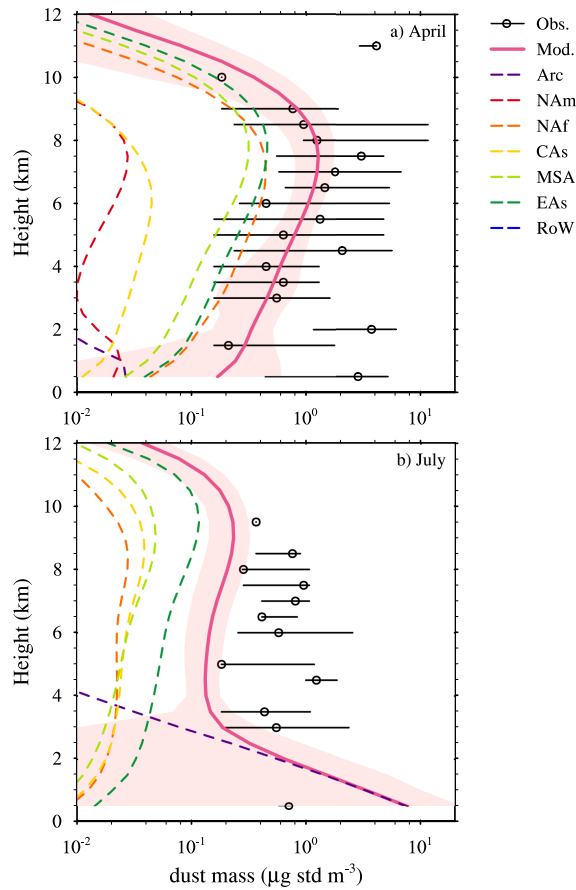
Formatted: Font: Not Bold

Formatted: Font: Not Bold

Formatted: Font: Not Bold

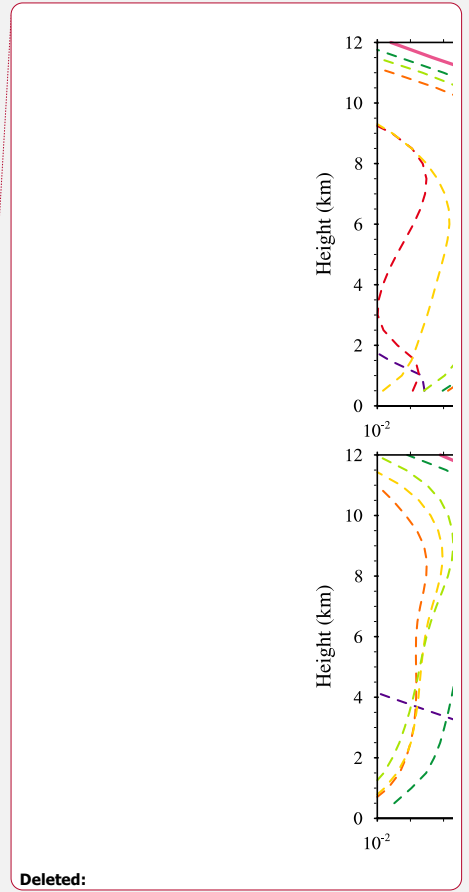
Formatted: Font: Not Bold

1156



1158

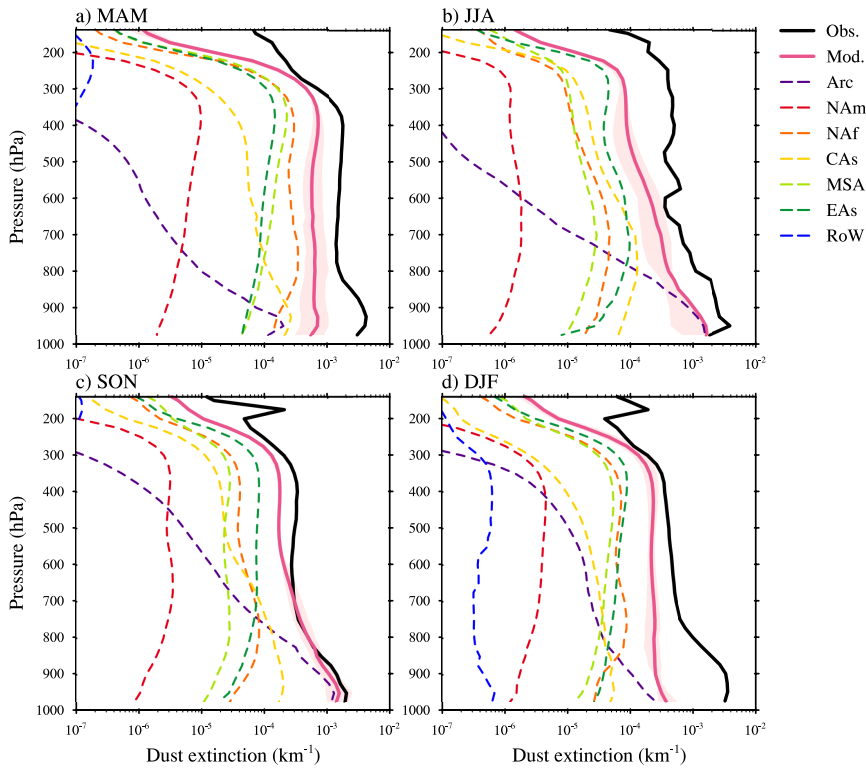
1159 **Figure 4.** Comparison of vertical dust concentrations from ARCTAS flight observations (Jacob et
 1160 al., 2010) (black circle) and CTRL simulation (pink solid line) in a) April and b) July. We show
 1161 median values for observations at each level. The maximum and minimum of the measurements
 1162 at each level are shown by black lines. Contributions from the seven tagged sources in CTRL are
 1163 shown by colored dashed lines. The ARCTAS dust mass concentrations are derived from measured
 1164 calcium and sodium concentrations. The measurements data are processed using the same method
 1165 as Breider et al. (2020). Briefly, we assume a calcium to dust mass ratio of 6.8% and further correct
 1166 the calcium concentrations for sea salt by assuming a calcium to sodium ratio of 4%. Only
 1167 measurements obtained north of 60°N are used for the analyses. The low-altitude observations
 1168 near Fairbanks, Barrow, and Prudhoe Bay are removed. Also, data from below 1 km on 1, 4, 5, 9



Formatted: Heading 1, Left, Line spacing: single
 Formatted: Font: Not Bold

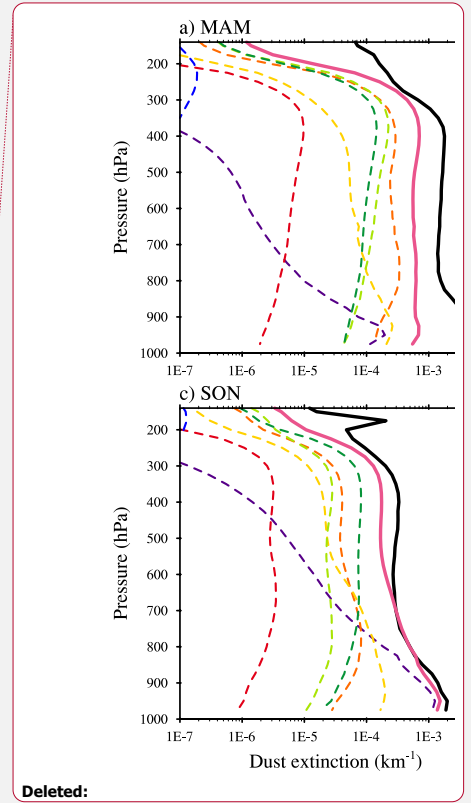
1170 July is removed to exclude the influence of wildfire. The ARCTAS flight campaign was conducted
1171 in 2008, while the modeled vertical profiles are averaged for each April and July from 2007 to
1172 2011, respectively. Following Groot Zwaafink et al. (2016), the simulation profiles are averaged
1173 for the regions north of 60°N and 170°W to 35°W in April and 135°W to 35°W in July. Also, the
1174 observations have a cut-off size of 4 μm and thus is only compared with simulated dust
1175 concentrations in the same size range. The pink shade on each panel represents the standard
1176 deviation with respect to time and space for the simulated total dust concentrations.

1177



1178

1179 **Figure 5.** Comparison of seasonal CALIPSO retrieved (Luo et al., 2015a, b) (black solid line) and
 1180 model simulated (pink solid line; with pink shade representing year-to-year variability) dust
 1181 extinction vertical profiles in the Arctic. Contributions from seven tagged sources are shown by
 1182 colored dashed lines. The CALIPSO retrieval is for the year 2007 to 2009, while the model is
 1183 averaged over the same years.



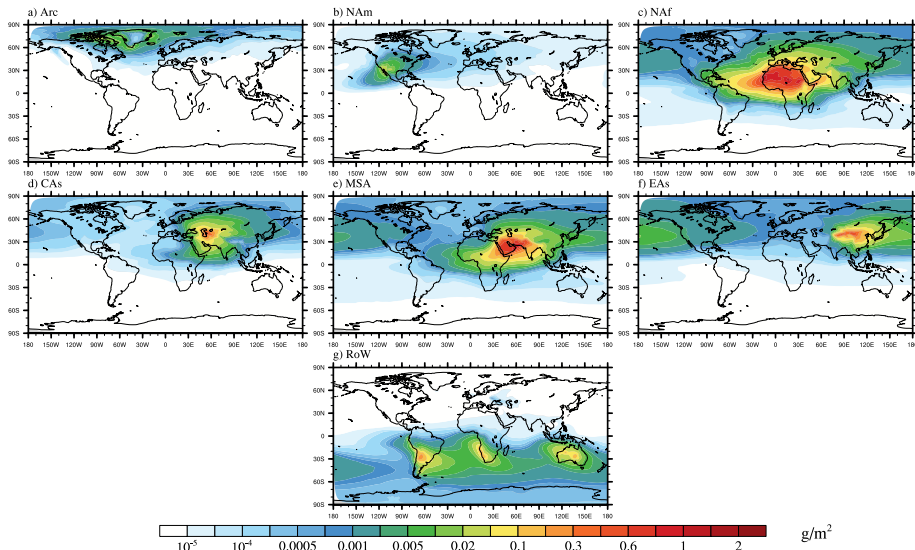
Deleted:

Formatted: Heading 1, Left, Line spacing: single

Formatted: Font: Not Bold

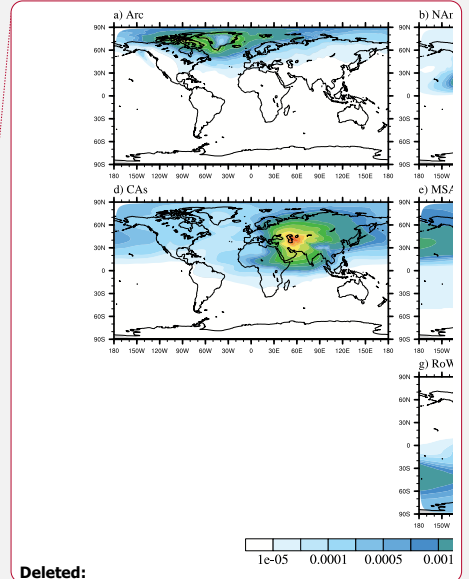
Formatted: Font: Not Bold

Deleted: Page Break



1186

1187 **Figure 6.** Spatial distribution of annual mean (year 2007 to 2011) dust column burdens for various
 1188 tagged sources.



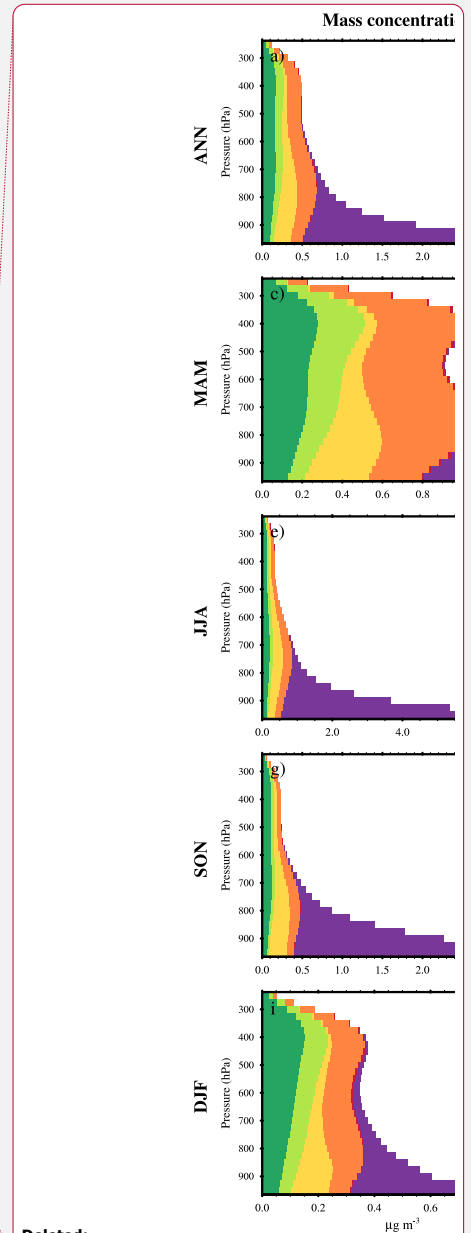
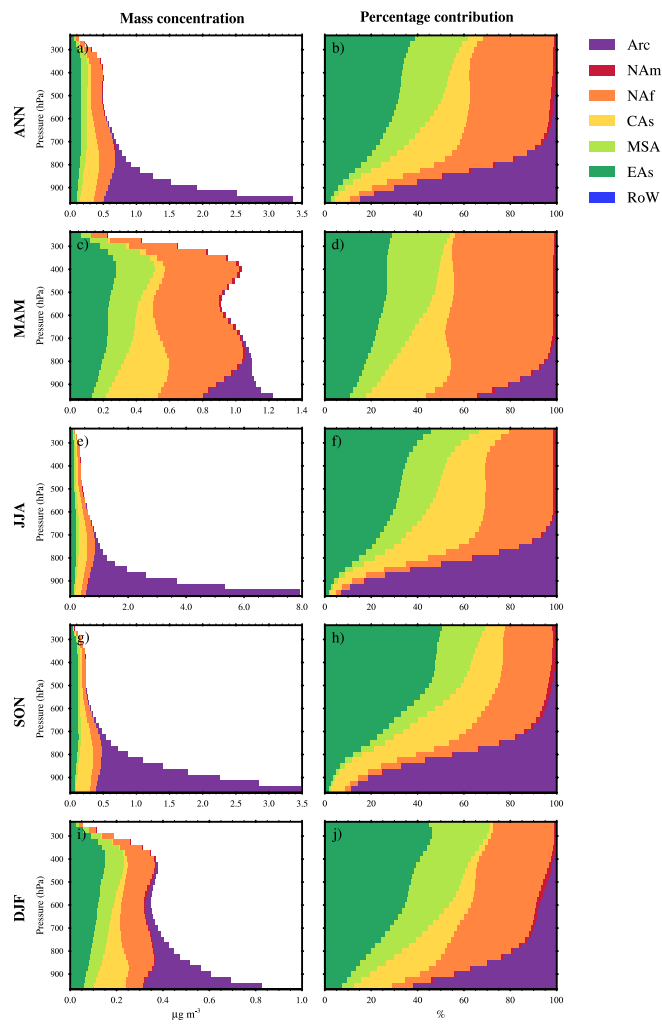
Deleted:

Formatted: Font: Not Bold

Formatted: Heading 1, Line spacing: single

Deleted: Global

Formatted: Font: Not Bold



Deleted:

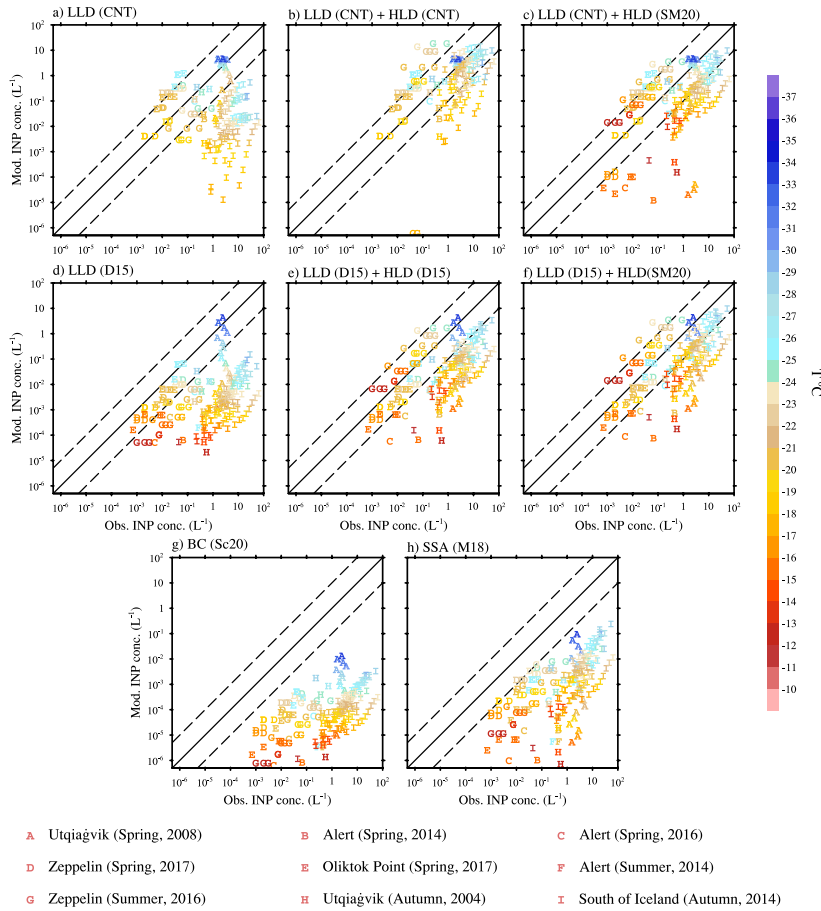
Formatted: Heading 1, Left, Line spacing: single

Formatted

... [1]

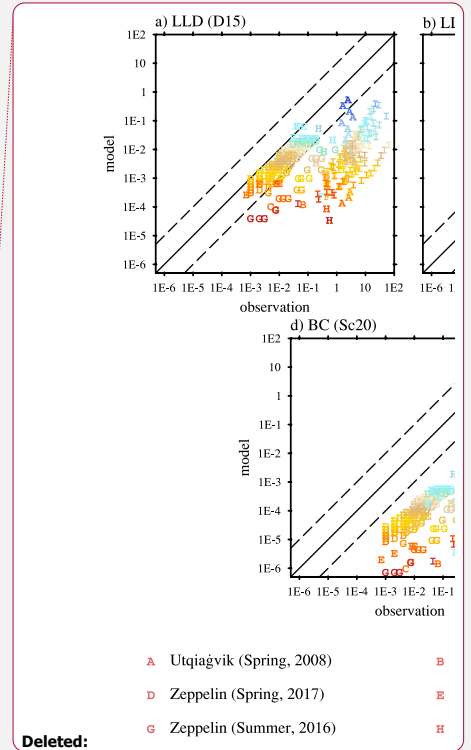
1191

1192 **Figure 7.** Annual and seasonal mean (year 2007 to 2011) Arctic vertical dust concentrations (left
 1193 panel) and percentage contributions from tagged sources (right panel). Different tagged sources
 1194 are classified by different colors.



1197

1198 **Figure 8.** Comparison of predicted versus observed INP concentrations in the Arctic. The
 1199 predicted INP concentrations are derived from a) LLD using classical nucleation theory (CNT), b)
 1200 LLD and HLD, both using CNT, c) LLD using CNT, and HLD using Sanchez-Marroquin et al
 1201 (2020; SM20), e) LLD using DeMott et al. (2015; D15), d) LLD and HLD, both using D15, e)
 1202 LLD using D15 and HLD using SM20, f) BC using Schill et al. (2020; Sc20), and g) SSA using
 1203 McCluskey et al. (2018; M18). SSA includes both marine organic aerosol and sea salt. Nine INP
 1204 datasets are classified by symbol “A” to “I”, the color of which represents the temperature reported
 1205 in the observations. The observations for datasets “A”, “C”, “E”, “H” are monthly mean values.
 1206 Samples for datasets “D”, “G”, “I” are selected randomly and only 15% of them are plotted. Details
 1207 of each campaign are summarized in Table 3. The modelled INP concentrations are diagnosed



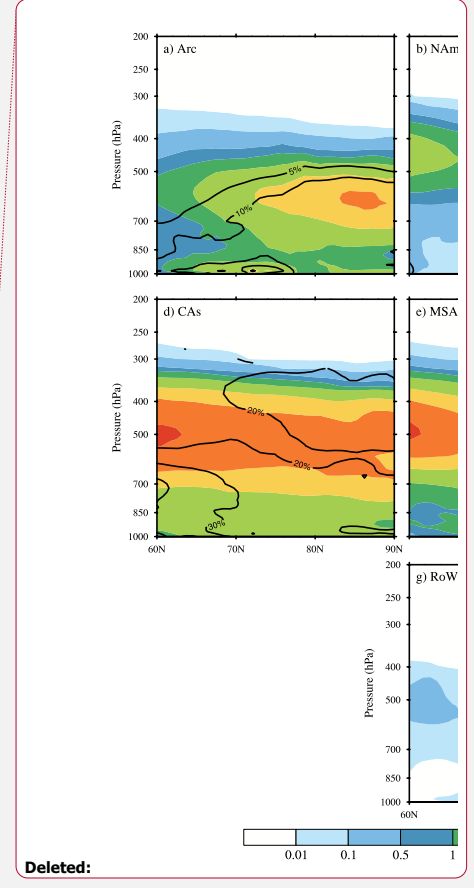
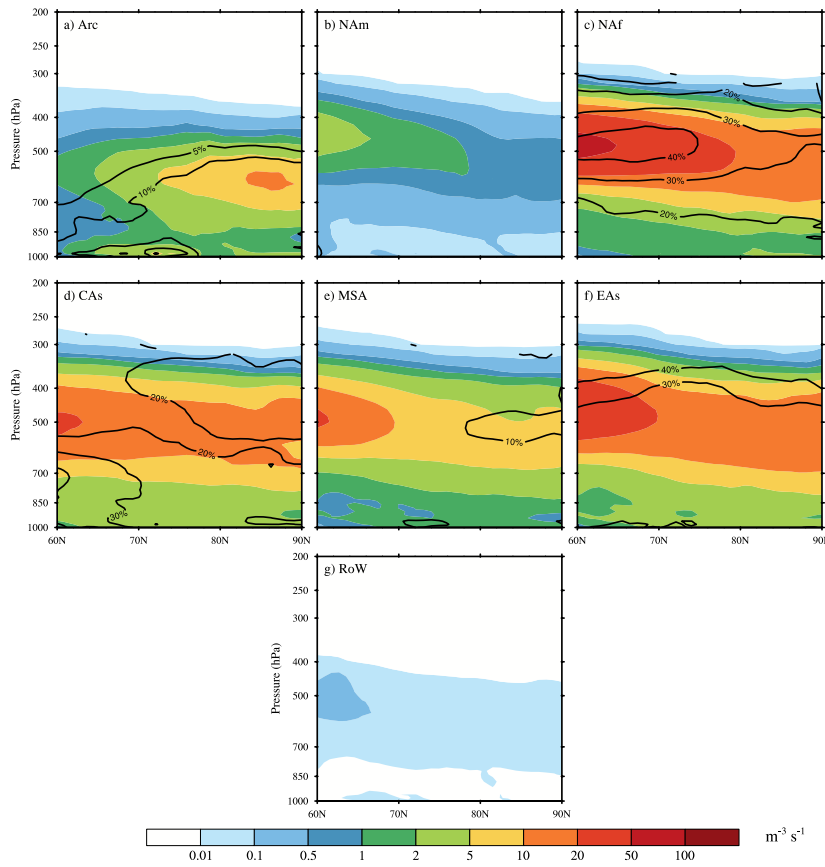
Deleted:

- Formatted: Font: Not Bold
- Formatted: Heading 1, Left, Line spacing: single
- Deleted: DeMott et al. (2015; D15),
- Formatted: Font: Not Bold
- Deleted: D15
- Deleted: D15
- Formatted: Font: Not Bold
- Deleted: d
- Formatted: Font: Not Bold
- Deleted: e
- Formatted: Font: Not Bold
- Deleted: observed temperature. Details of each campaign are summarized in Table 3.

1216 using the observed temperatures and monthly averaged aerosol properties of the corresponding
1217 month from year 2007 to 2011. The INP concentrations for CNT are defined as the CNT immersion
1218 freezing rate integrated by 10 s, following Hoose et al. (2010) and Wang et al. (2014). Solid line
1219 in each panel represents 1:1 comparison, while dashed lines outline one order of magnitude
1220 differences. The unit for INP concentration is L^{-1} .

1221

Formatted: Font: Not Bold

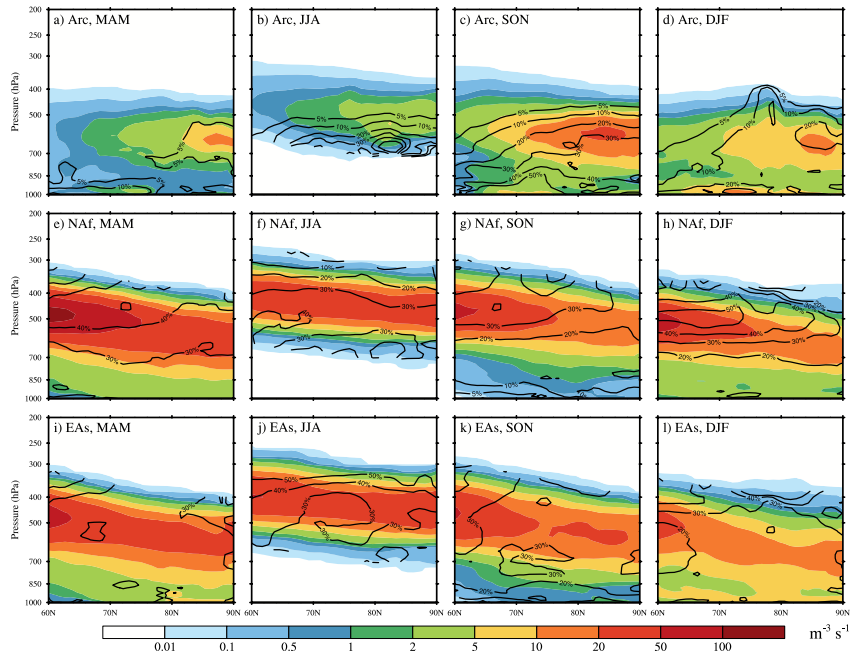


1222

1223 **Figure 9.** Annual and zonal mean (year 2007 to 2011) ambient mixed-phase cloud immersion
 1224 freezing rates (unit: $\text{m}^{-3} \text{s}^{-1}$) in the Arctic ($60\text{-}90^\circ\text{N}$) for the seven dust sources. Black contours are
 1225 the percentage contributions from each dust source to the total immersion freezing rate.

1226

- Formatted: Font color: Black
- Formatted: Font: Not Bold, Font color: Black
- Formatted: Font: Not Bold, Font color: Black
- Formatted: Heading 1, Left, Line spacing: single
- Formatted: Font: Not Bold
- Formatted: Font: Not Bold, Font color: Black



1228

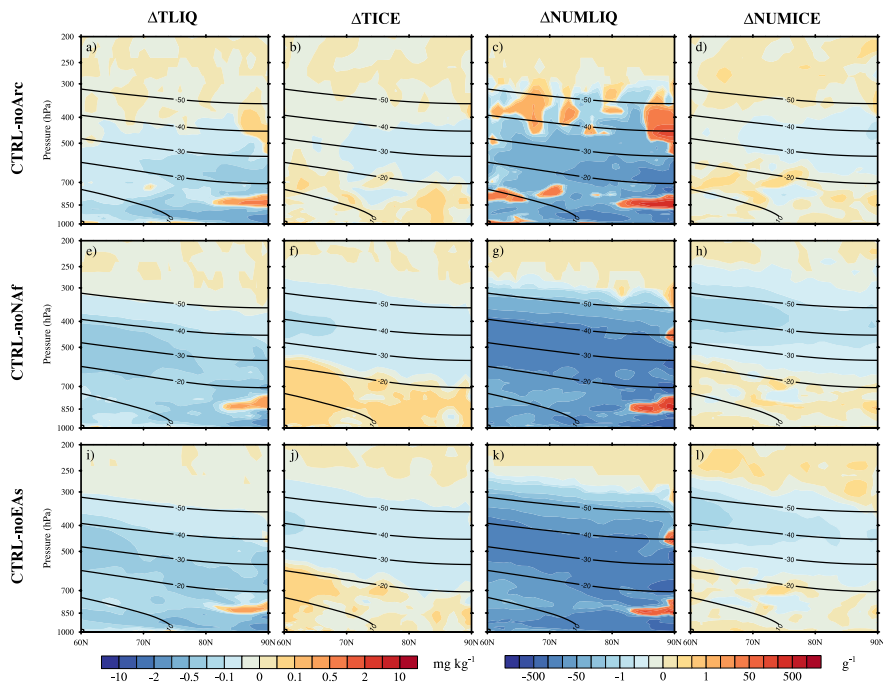
1229 **Figure 10.** Seasonal variations (year 2007 to 2011) of the mixed-phase clouds immersion freezing
 1230 rates (unit: $\text{m}^{-3} \text{s}^{-1}$) over the Arctic for dust emitted from the Arctic (top panel), North Africa
 1231 (middle panel), and East Asia (bottom panel). Black contours are the percentage contributions
 1232 from each dust source to the total immersion freezing rate in the corresponding season.

1233

Formatted: Heading 1, Left, Line spacing: single

Formatted: Font: Not Bold

Formatted: Font: Not Bold



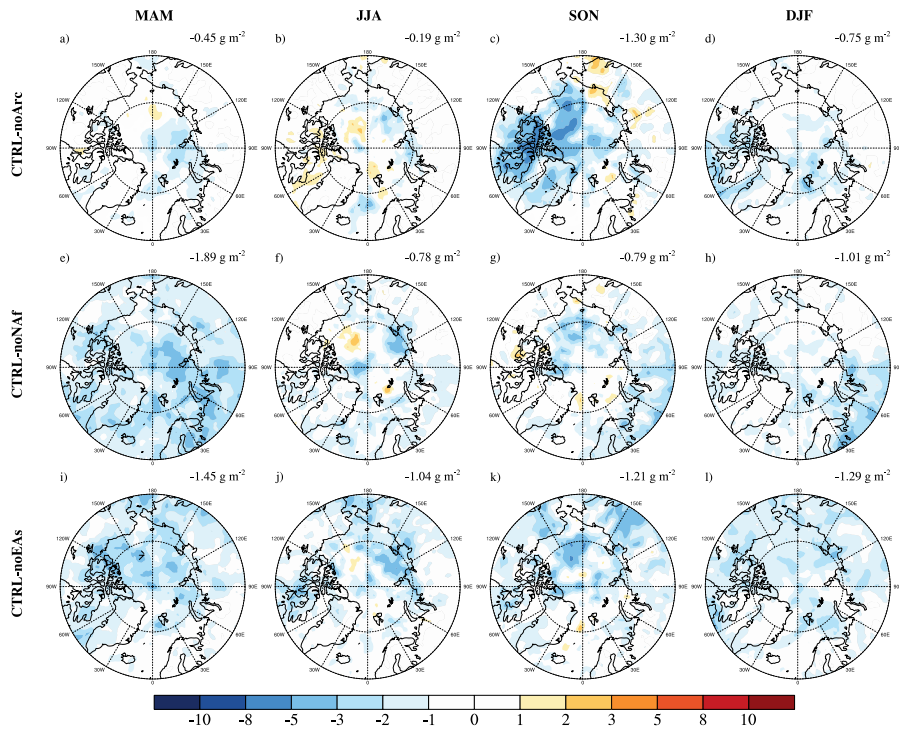
1234

1235 **Figure 11.** Annual and zonal mean differences (year 2007 to 2011) in total liquid water mass
 1236 mixing ratio (TLIQ), total ice mixing ratio (TICE), cloud droplet number concentration
 1237 (NUMLIQ), and cloud ice number concentration (NUMICE) in the Arctic. Black contours are
 1238 zonal averaged temperatures in °C. Top, middle, and bottom panels show the differences between
 1239 CTRL and noArc, noNAf, and noEAs, respectively.

Formatted: Heading 1, Left, Line spacing: single

Formatted: Font: Not Bold

Formatted: Font: Not Bold



1240

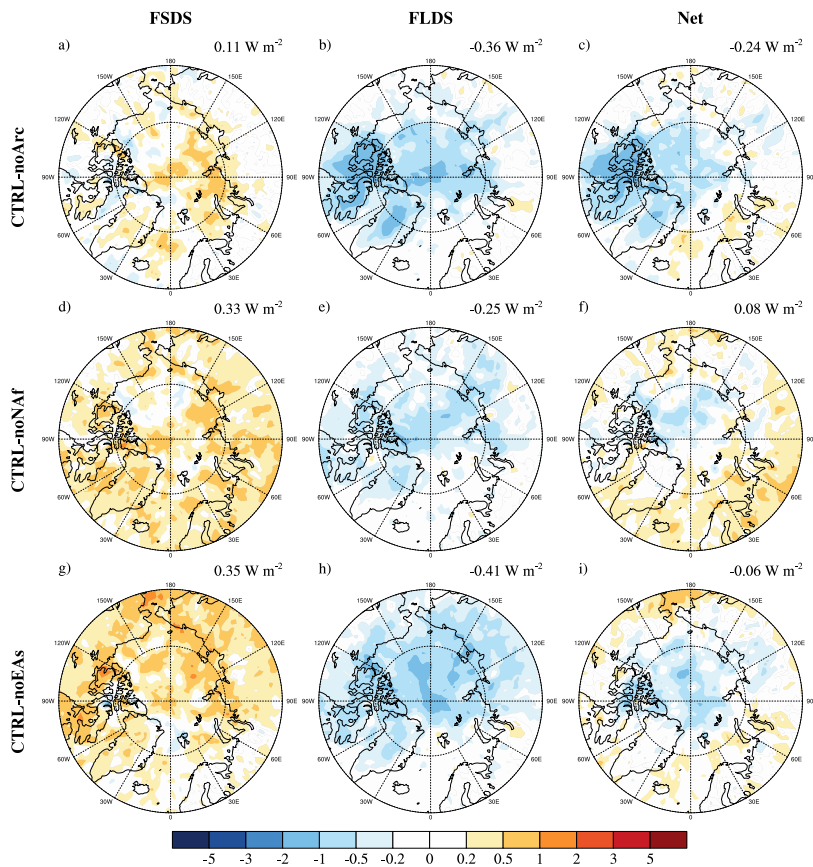
1241 **Figure 12.** Seasonal changes (year 2007 to 2011) in LWP (unit: g m^{-2}) caused by dust INPs from
 1242 the Arctic (top panel), North Africa (middle panel), and East Asia (bottom panel). The numbers
 1243 are averaged LWP differences in the Arctic.

1244

Formatted: Heading 1, Left, Line spacing: single

Formatted: Font: Not Bold

Formatted: Font: Not Bold



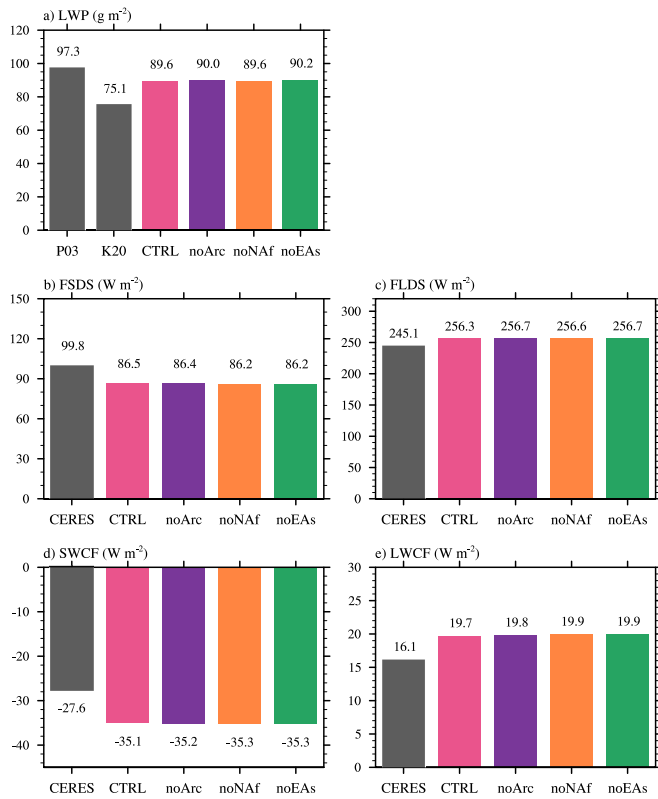
1245

1246 **Figure 13.** Changes in annual mean (year 2007 to 2011) downwelling radiative fluxes at the
 1247 surface (unit: W m^{-2}) caused by dust INPs from the Arctic (top panel), North Africa (middle panel),
 1248 and East Asia (bottom panel). Left, middle, and right panels are downwelling shortwave (FSDS),
 1249 longwave (FLDS), and net (FSDS + FLDS) radiative fluxes, respectively. The numbers are
 1250 averaged radiative flux differences in the Arctic.

1251

Formatted: Font: Not Bold

Formatted: Font: Not Bold



1252

1253 **Figure 14.** a) Annual mean Arctic averaged LWP over ocean for the MODIS observations (2007-
 1254 2009) and the four simulations (2007-2008). Two MODIS datasets are used, including the standard
 1255 product (Platnick et al., 2003; P03) and an improved one (Khanal et al., 2020; K20). The MODIS
 1256 simulator is used to calculate the simulated LWP. b) - e) Annual mean Arctic averaged b) FSDS,
 1257 c) FLDS, d) SWCF, and e) LWCF for the CERES observation (2007-2011) and the four
 1258 simulations (2007-2011).

1259

Formatted: Font: Bold, English (UK)
 Formatted: Left, Line spacing: single

Font: Not Bold

Font: Not Bold